Novel Structure-Exploiting Techniques Based Delay-Dependent Stability Analysis of Multi-Area LFC with Improved Numerical Tractability

Li Jin, *Student Member, IEEE,* Yong He, *Senior Member, IEEE,* Chuan-Ke Zhang, *Senior Member, IEEE,* Xing-Chen Shangguan, *Student Member, IEEE,* Lin Jiang, *Member, IEEE,* and Min Wu, *Fellow, IEEE*

***Abstract*—Time-domain indirect methods based on Lyapunov stability theory and linear matrix inequality techniques (LMIs) have been applied for delay-dependent stability analysis of large-scale load frequency control (LFC) schemes. This paper aims to enhance the numerical tractability of large-scale LMIs by exploiting the special characteristics of the LFC loops. First, in the typical LFC model, only a few delayed states that are directly influenced by transmission delays are distinguished from other normal system states. Hence, an improved reconstruction model is formed, based on which the delay-dependent stability condition is established with the decreased order of the LMIs and decision variables. Then, to further improve the numerical tractability of the developed stability criterion, all weighting matrices required in the augmented Lyapunov functional are enforced to have structural restrictions by proposing an extended symmetry-exploiting technique. Case studies show that the method proposed in this paper significantly improves the calculation efficiency of stability criterion established for multi-area power systems at the cost of only a minor reduction in computational accuracy.**

***Index Terms*—Load frequency control, linear matrix inequality, numerical tractability, model reconstruction, symmetry-exploiting technique.**

I. Introduction

Load frequency control (LFC) plays a significant role in power systems by maintaining their frequency and power interchanges with neighbourhood areas at scheduled values [1]. The LFC schemes utilize communication networks to transmit information between the control centre and remote generator units, inevitably inducing time delays [2]. These delays degrade the dynamic performance of power systems and can even threaten their safe operation [3], [4]. Hence, it is essential to evaluate the influence of time delays on the power system stability in order to design proper controllers and eliminate the adverse effects of time delays [5]. The previous research can be classified into two categories, i.e., frequency-domain direct methods and time-domain indirect methods [6].

Frequency-domain direct methods can obtain the accurate delay margins for a power system with constant time delays, e.g., a single-area LFC scheme with constant delay [7] and multi-area LFC schemes with equal time delays [8]. The development of smart grid technologies requires increased usage of open communication networks where random delays or time-varying delays will inevitably occur [9], [10]. To address these delays, the time-domain indirect methods based on Lyapunov stability theory and linear matrix inequality techniques (LMIs) have been an alternative approach [11]. Such approaches are used to compute the delay margins approximately by constructing augmented Lyapunov functionals and/or estimating their derivatives with conservatism-reduced inequalities [12], [13] and to design the LFC controllers [14], [15].

In addition to calculation accuracy, the heavy computational burden is another issue to analyze the delayed power system with these two groups of approaches since the real-world power system is high-dimensional. Based on the frequency-domain methods, many computational frameworks have been presented for efficient eigen-analysis by exploiting model sparsity [16], [17] and partial eigenvalue solving methods [18]. Moreover, considering the time-domain LMIs-based methods, since the state-of-art LMI solvers have the limited capability to solve large-scale LMIs, previous studies have sought to reduce the scale of the system model and the order of LMIs together with the number of decision variables [19].

For instance, in [20], stability criteria are proposed with a lower number of decision variables to reduce the calculation time; however, these criteria are not especially established for the LFC problem. Many special features of the LFC scheme have not been fully considered in this method. By considering the sparse feature of coefficient matrices in the system model, Yu et al. attempt to decompose the system model into a delay-free part and a delay-related part [21]. Then, the Lyapunov functional can be constructed mainly based on the relatively low-order delay-related part. Note that this method uses too strict rules for finding time-delayed

This work is supported by the National Natural Science Foundation of China under Grants 61973284, 62022074, and 61873347, the Hubei Provincial Natural Science Foundation of China under Grants 2019CFA040, the 111 Project under Grant B17040, and the Fundamental Research Funds for National Universities, China University of Geosciences (Wuhan). (*Corresponding author: Lin Jiang.*)

L. Jin, and X.C. Shangguan are with the School of Automation, China University of Geosciences, Wuhan, 430074, China, and with Hubei Key Laboratory of Advanced Control and Intelligent Automation for Complex Systems, Wuhan, 430074, China, and with Engineering Research Center of Intelligent Technology for Geo-Exploration, Ministry of Education, Wuhan, 430074, China, and also with the Department of Electrical Engineering and Electronics, University of Liverpool, Liverpool, L69 3GJ, United Kingdom. (Email: jinli@cug.edu.cn; star@cug.edu.cn).

Y. He, C.K. Zhang, and M. Wu are with the School of Automation, China University of Geosciences, Wuhan, 430074, China, and with Hubei Key Laboratory of Advanced Control and Intelligent Automation for Complex Systems, Wuhan, 430074, China, and also with Engineering Research Center of Intelligent Technology for Geo-Exploration, Ministry of Education, Wuhan, 430074, China. (Email: heyong08@cug.edu.cn; ckzhang@cug.edu.cn; wumin@cug.edu.cn).

L. Jiang is with the Department of Electrical Engineering and Electronics, University of Liverpool, Liverpool, L69 3GJ, United Kingdom. (Email: ljiang@liverpool.ac.uk).

variables to decompose the LFC model equipped with a PID-type controller. Thus, the authors in [22] propose an increasing slack method to reconstruct the system model based on which the established stability criterion has enhanced computational efficiency. The calculation accuracy is guaranteed by choosing a Lyapunov functional whose augmented part has integral terms containing the time delays in the adjacent regions of the power system. Nevertheless, this reconstructed method shows a strong dependence on the values of the coefficient matrices. Furthermore, the utilization of augmented-type Lyapunov functional generates an additional calculation burden for large-scale LMIs. In [19], the symmetry structure of the LFC loops is exploited to restrict the weighting matrices of Lyapunov functionals such that the solvability of LMIs is enhanced. However, this technique is only subject to the weighting matrix contained in the non-integral term of the Lyapunov functional and is not beneficial for other integral parts of the functional.

This paper proposes an improved reconstructed model and an extended symmetry-exploiting technique for the delay-dependent stability analysis of large-scale LFC systems such that the computation burden of time-domain-based LMIs is greatly reduced. The contributions of this paper are summarized as follows.

- An improved reconstruction model is presented by decomposing the system states into two parts, i.e., the delay-related states and delay-free states, based on which the stability condition is established with enhanced numerical tractability. The authors in [22] focus on the sparsity and the non-zero elements of coefficient matrices whose values significantly affect the determination of delayed states. Whereas, by considering the mechanism of the LFC schemes in this paper, the relatively small number of states that are influenced directly by remote transmission delays are separated from other normal states.
- An extended symmetry-exploiting technique is proposed to structurally address all weighting matrices required in the augmented Lyapunov functional, while the technique in [19] can only deal with one component in the simple Lyapunov functional. Thus, the number of decision variables contained in the large-scale LMIs is greatly reduced.
- To validate the effectiveness of the proposed method, case studies are carried out on both single-area and three-area LFC schemes. Compared with previous studies, the developed condition that benefits from the improved reconstruction method and the extended symmetry-exploiting technique shows a great improvement in calculation efficiency at a minor cost of calculation accuracy.

The remainder of this paper is organized as follows. Section II presents the dynamic model of the multi-area LFC schemes and an improved reconstructed method. Then, based on the reconstructed model, an augmented-type Lyapunov functional is employed to establish a stability criterion. Section III realizes the extended structure-exploiting technique by considering the symmetry feature of the LFC schemes. In Section IV, case studies are carried out on the single-area and three-area LFC schemes to demonstrate the effectiveness of proposed technique. Finally, Section V states the conclusions.

II. Multi-area LFC scheme and Delay-dependent Stability Analysis

The dynamic model of multi-area LFC schemes in [20] is initially recalled. Then, an improved reconstructed technique is proposed, based on which the stability criterion can be obtained with increased computational efficiency.

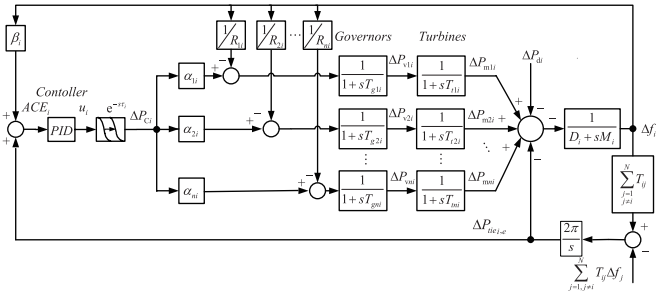

Fig. 1. Structure of control area i in the multi-area of LFC scheme.

TABLE I
Notations

Δf_i	Deviation of frequency
$\Delta P_{tie-i,e}$	Deviation of tie-line power exchange
ΔP_{mni}	Deviation of generator mechanical output
ΔP_{vni}	Deviation of valve position
M_i	Moment of inertia of generator unit
D_i	Generator unit damping coefficient
T_{gni}	Time constant of non-reheat turbine speed governor
T_{tni}	Time constant of non-reheat turbine
R_{ni}	Speed drop
β_i	Frequency bias factor
α_{ni}	Ramp rate factor
T_{SG}	Time constant of reheat turbine speed governor
K_R	Coefficient of reheater steam
T_R	Time constant of turbine reheater
T_T	Time constant of reheat turbine
T_{GH}	Time constant of main servo
T_{RS}	Reset time of hydro turbine speed governor
T_{RH}	Time constant of transient droop
T_W	Time constant of penstock water

A. Dynamic model of the multi-area LFC scheme

The structure of area i is shown in Fig. 1. Table I gives the notations employed for the ith area of the LFC system. The exponential block $e^{-s\tau_i}$ shows the delays arising in the communication channels [23]; each area of the LFC schemes is assumed to equip n generators installed with non-reheat turbines and a PID controller.

The area control error (ACE) of area i is defined as

$$ACE_i = \beta_i \Delta f_i + \Delta P_{tie_i,e} \tag{1}$$

and a PID-type LFC controller is designed as

$$u_i(t) = -K_{Pi} ACE_i - K_{Ii} \int ACE_i dt - K_{Di} \frac{dACE_i}{dt} \tag{2}$$

where K_{Pi}, K_{Ii} and K_{Di} are the proportional, integral and differential gains, respectively. Here, the closed-loop model of the LFC scheme is recalled from [20].

$$\dot{x}(t) = Ax(t) + \sum_{i=1}^{N} A_{\mathrm{d}i} x(t-\tau_i) + B_{\mathrm{w}}\omega \tag{3}$$

where

$$x = [\bar{x}_1^T, \bar{x}_2^T, \ldots, \bar{x}_n^T]^T, \quad \bar{x}_i = [\hat{x}_i^T, \int y_i^T]^T, \quad y_i = ACE_i$$

$$\hat{x}_i = [\Delta f_i, \Delta P_{tie_i,e}, \Delta P_{m1i}, \ldots, \Delta P_{mni}, \Delta P_{v1i}, \ldots, \Delta P_{vni}]^T$$

$$A=\begin{bmatrix}\bar{A}_{11}&\cdots&\bar{A}_{1N}\\ \vdots&\ddots&\vdots\\ \bar{A}_{N1}&\cdots&\bar{A}_{NN}\end{bmatrix}, A_{\mathrm{d}i}=\begin{bmatrix}0_{(i-1)(2n+2)\times N(2n+2)}\\ \bar{A}_{\mathrm{d}i1}\ \bar{A}_{\mathrm{d}i2}\cdots\bar{A}_{\mathrm{d}iN}\\ 0_{(N-i)(2n+2)\times N(2n+2)}\end{bmatrix}$$

$$B_{\mathrm{w}}=\mathrm{diag}\{\bar{B}_{\mathrm{w}1},\cdots,\bar{B}_{\mathrm{w}N}\},\ \omega=\mathrm{diag}\{\omega_1,\cdots,\omega_N\}$$

$$\bar{A}_{\mathrm{d}ii}=-\bar{B}_iK_i\bar{C}_i,\ \bar{A}_{\mathrm{d}ij}=-\bar{B}_iK_i\bar{C}_{ij},\ \bar{B}_{\mathrm{w}i}=\bar{F}_i-\bar{B}_iK_i\bar{D}_i$$

$$\bar{A}_{ii}=\begin{bmatrix}A_i&0\\ C_i&0\end{bmatrix},\ \bar{A}_{ij}=\begin{bmatrix}A_{ij}&0\\ 0&0\end{bmatrix},\ \bar{B}_i=\begin{bmatrix}B_i\\ 0\end{bmatrix},\ \bar{F}_i=\begin{bmatrix}F_i\\ D_i\end{bmatrix}$$

$$\bar{C}_i=\begin{bmatrix}C_i&0\\ 0&1\\ C_iA_i&0\end{bmatrix},\bar{C}_{ij}=\begin{bmatrix}0&0\\ 0&0\\ C_iA_{ij}&0\end{bmatrix},\bar{D}_i=\begin{bmatrix}D_i\\ 0\\ C_iF_i\end{bmatrix}$$

$$A_i=\begin{bmatrix}A_{11i}&A_{12i}&0_{2\times n}\\ 0_{n\times 2}&A_{22i}&A_{23i}\\ A_{31i}&0_{n\times n}&A_{33i}\end{bmatrix},A_{ij}=\begin{bmatrix}0&0&0_{1\times 2n}\\ 2\pi T_{ij}&0&0_{1\times 2n}\\ 0_{2n\times 1}&0_{2n\times 1}&0_{2n\times 2n}\end{bmatrix}$$

$$A_{11i}=\begin{bmatrix}-\frac{D_i}{M_i}&-\frac{1}{M_i}\\ 2\pi\sum_{j=1,j\neq i}^{N}T_{ij}&0\end{bmatrix},A_{12i}=\begin{bmatrix}\frac{1}{M_i}&\cdots&\frac{1}{M_i}\\ 0&\cdots&0\end{bmatrix}$$

$$A_{22i}=-A_{23i}=-\mathrm{diag}\left\{\frac{1}{T_{t1i}},\cdots,\frac{1}{T_{tni}}\right\}$$

$$A_{31i}=-\begin{bmatrix}\frac{1}{R_{1i}T_{t1i}}&\cdots&\frac{1}{R_{ni}T_{tni}}\\ 0&\cdots&0\end{bmatrix}^T$$

$$A_{33i}=-\mathrm{diag}\left\{\frac{1}{T_{g1i}},\cdots,\frac{1}{T_{gni}}\right\}$$

$$B_i=\begin{bmatrix}0_{2\times 1}\\ 0_{n\times 1}\\ B_{3i}\end{bmatrix},B_{3i}=\left[\frac{\alpha_{1i}}{T_{g1i}},\cdots,\frac{\alpha_{ni}}{T_{gni}}\right]^T,F_i=\begin{bmatrix}-\frac{1}{M_i}\\ 0_{(2n+1)\times 1}\end{bmatrix}$$

$$C_i=[\beta_i,1,0_{1\times 2n}],\beta_i=\sum_{j=1}^{n}\frac{1}{R_{ji}}+D_i.$$

Similarly, in the analysis of the asymptotical stability of (3), we consider the following disturbance-free model:

$$\dot{x}(t)=\sum_{i=0}^{N}A_ix(t-\tau_i) \tag{4}$$

where $A_0=A$ and $A_i\in\{A_{\mathrm{d}1},A_{\mathrm{d}2},\ldots,A_{\mathrm{d}N}\}$ are obtained by reordering the time delays with $0=\tau_0\leq\tau_1\leq\ldots\leq\tau_N$.

B. Improved reconstructed model

Based on Fig. 1, the state variables selected for area i have the following relationships:

$$\begin{aligned}&\Delta\dot{f}_i(t)=\lambda(\Delta P_{mki}(t),\Delta P_{di}(t),\Delta P_{tie_i,e}(t))\\ &\Delta\dot{P}_{tie_i,e}(t)=h(\Delta f_i(t),\Delta f_j(t))\\ &\Delta\dot{P}_{mki}(t)=g(\Delta P_{mki}(t),\Delta P_{vki}(t))\\ &\Delta\dot{P}_{vki}(t)=f(\Delta f_i(t),\Delta P_{vki}(t))+\chi(\Delta f_i(t-\tau_i),\Delta P_{tie_i,e}(t-\tau_i))\end{aligned} \tag{5}$$

where $k=1,2,\ldots,n$, and $\lambda(\cdot),h(\cdot),g(\cdot),f(\cdot)$ and $\chi(\cdot)$ are appropriate functions defined in Appendix I. In area i, only state variables $\Delta\dot{P}_{vki}(t)$ are affected by the delayed states directly, which is also the case for area j. Therefore, we separate variables $\Delta\dot{P}_{vki}(t),k=1,2,\ldots,n,i=1,2,\ldots,N$ from the state vector x and place them in $x_2\in R^{n_2}$. Meanwhile, let $x_1\in R^{n_1}$ consist of the rest of the state variables in x. Through elementary row operation on system (4), we can conveniently obtain

$$\begin{cases}\dot{x}_1(t)=a_1x_1(t)+a_2x_2(t)\\ \dot{x}_2(t)=a_3x_1(t)+a_4x_2(t)+\sum_{i=0}^{N}a_{\mathrm{d}i}x_1(t-\tau_i)\end{cases} \tag{6}$$

where $\begin{bmatrix}a_1&a_2\\ a_3&a_4\end{bmatrix}$ and $\begin{bmatrix}0&0\\ \sum_{i=0}^{N}a_{\mathrm{d}i}&0\end{bmatrix}$ are equal to the values of A_0 and $\sum_{i=1}^{N}A_i$ after row operations, respectively.

The difference between the methods in [22] and this paper is how the delayed state vector x_1 and delay-free state vector x_2 are defined. Based on the structure of the LFC scheme and formulations (5), this paper regards x_2 as the combination of the states about the derivation of the valve positions while letting the rest of the states in x be x_1. This decomposition is determined only if the number of the generators used in the LFC schemes is given. For example, considering the single-area LFC scheme with n installed generators, the total number of states in the LFC system is $2n+2$ including n states about the derivations of the valve position. Therefore, the dimension of the second part in the reconstructed model is n, while the first part has the order of $n+2$, completing the procedure of composition. However, in [22], the delayed states are found by exploiting the non-zero elements in coefficient matrix $\sum_{i=1}^{N}A_i$, i.e., the reconstructed method must change when different values of the PID-type controllers are given. When analyzing the stability of the LFC schemes equipped with various PID controllers, the reconstructed model in [22] is more complicated than the method proposed in this paper.

C. Delay-dependent stability criterion

As system (6) is used to investigate the delay-dependent stability analysis of multi-area LFC with enhanced computation efficiency, the following criterion is obtained to ensure the asymptotical stability of system (6).

Theorem 1. *For given scalars $\tau_i,i=0,1,...,N$, system (6) is globally asymptotically stable, if there exist symmetric positive matrices $P,U_i,Z_i,i=1,2,...,N$, such that the following LMI holds:*

$$\Pi=E_{2N}^TPE_{1N}+E_{1N}^TPE_{2N}+\sum_{i=1}^{N}\Theta_i<0 \tag{7}$$

where

$$\begin{aligned}\Theta_i&=e_i^TU_ie_i-e_{i+1}^TU_ie_{i+1}+(\tau_i-\tau_{i-1})^2e_{s1}^TZ_ie_{s1}\\ &\quad-E_i^T\mathrm{diag}\{Z_i,3Z_i\}E_i\\ E_{1N}&=\left[e_{s1}^T\ e_{s0}^T\ (e_1-e_2)^T\ \ldots\ (e_N-e_{N+1})^T\right]^T\\ E_{2N}&=\left[e_1^T\ e_0^T\ (\tau_1-\tau_0)e_{N+2}^T\ \ldots\ (\tau_N-\tau_{N-1})e_{2N+1}^T\right]^T\\ E_i&=\left[(e_i-e_{i+1})^T\ (e_i+e_{i+1}-2e_{N+1+i})^T\right]^T\\ e_{s1}&=a_1e_1+a_2e_0\\ e_{s0}&=a_3e_1+a_4e_0+\sum_{i=1}^{N}a_{\mathrm{d}i}e_{i+1}\\ e_i&=\left[0_{n_1\times(i-1)n_1},I_{n_1\times n_1},0_{n_1\times(2N+1-i)n_1},0_{n_1\times n_2}\right],i=1,2,...,2N+1\\ e_0&=\left[0_{n_2\times(2N+1)n_1},I_{n_2\times n_2}\right].\end{aligned}$$

Proof. We choose the following Lyapunov functional

$$\begin{aligned}V(t)&=\xi^T(t)P\xi(t)+\sum_{i=1}^{N}\int_{t-\tau_i}^{t-\tau_{i-1}}x_1^T(s)U_ix_1(s)ds\\ &\quad+\sum_{i=1}^{N}(\tau_i-\tau_{i-1})\int_{-\tau_i}^{-\tau_{i-1}}\int_{t+\theta}^{t}\dot{x_1}^T(s)Z_i\dot{x_1}(s)dsd\theta\end{aligned} \tag{8}$$

with $\xi^T(t)=\left[x_1^T(t),x_2^T(t),\int_{t-\tau_1}^{t-\tau_0}x_1^T(s)ds,\ldots,\int_{t-\tau_N}^{t-\tau_{N-1}}x_1^T(s)ds\right]$, $P\in R^{((N+1)n_1+n_2)\times((N+1)n_1+n_2)}$, $U_i\in R^{n_1\times n_1}$, and

$Z_i \in R^{n_1 \times n_1}$ as the matrices to be determined.

Then, by calculating the derivative of the Lyapunov functional (8) along equation (6), we have

$$\dot{V}(t) = 2\xi^T(t)P\dot{\xi}(t) + \sum_{i=1}^{N} x_1^T(t-\tau_{i-1})U_i x_1(t-\tau_{i-1}) - \sum_{i=1}^{N} x_1^T(t-\tau_i)U_i x_1(t-\tau_i) + \sum_{i=1}^{N}(\tau_i-\tau_{i-1})^2 \dot{x}_1^T(t)Z_i\dot{x}_1(t) - \sum_{i=1}^{N}(\tau_i-\tau_{i-1})\int_{t-\tau_i}^{t-\tau_{i-1}} \dot{x}_1^T(s)Z_i\dot{x}_1(s)ds \quad (9)$$

Employing Wirtinger-based inequality (14) to estimate the integral terms in (9) yields

$$\dot{V}(t) \leq \varphi^T(t)\Pi\varphi(t)$$

where $\varphi^T(t) = \Big[x_1^T(t), x_1^T(t-\tau_1), \cdots, x_1^T(t-\tau_N), \int_{t-\tau_1}^{t-\tau_0}\frac{x_1^T(s)}{\tau_1-\tau_0}ds, \cdots, \int_{t-\tau_N}^{t-\tau_{N-1}}\frac{x_1^T(s)}{\tau_N-\tau_{N-1}}ds, x_2^T(t)\Big]$, and Π is defined in (7). Thus, the LMI-based condition in Theorem 1 leads to $V(t) > 0$ and $\dot{V}(t) \leq -\varepsilon \left\|x(t)\right\|^2$ for a sufficient small scalar $\varepsilon > 0$, which guarantees the asymptotical stability of system (6).

III. Symmetry-exploiting delay-dependent stability analysis

This section provides a detailed description of the implementation of the extended symmetry-exploiting technique.

A. Extended symmetry-exploiting technique

As shown in Fig.1, the LFC control loops have symmetric structures and similar parameters for the generator units due to the similar specifications of the same type of power equipment installed in the same area. Therefore, to alleviate the computational burden of solving large-scale LMIs, the symmetry-exploited technique is presented in [19]. In detail, when the quadratic term x^TPx is constructed to form the first item in the Lyapunov functional, the weighting matrix $P \in R^{n_1+n_2}$ is appropriately restricted. Based on the fact that the "nature" of the state variable pair (κ_1, υ_1) is the same as that of the state variable pair (κ_2, υ_2), we can let $[P]_{\kappa_1\upsilon_1}$ and $[P]_{\kappa_2\upsilon_2}$ take the similar values with $\kappa_1, \upsilon_1, \kappa_2, \upsilon_2 \in \{1, \ldots, n_1+n_2\}$. For example, considering the single-area LFC scheme, since ΔP_{m1} and ΔP_{m2} have the same relations to Δf, the pairs of state variables can be $(1,3)$ and $(1,4)$.

It should be noted that with the exception of the weighting matrix P in the Lyapunov functional, the weighting matrices such as $U_i, Z_i, i = 1, 2, \ldots, N$ required by the integral terms are not restricted by the existing symmetry-exploited technique [19]. Moreover, the delay margins are determined to be an additional index for guiding the controller design such that the adverse effect of time delay is eliminated. Therefore, we have to reduce the conservatism of stability analysis. Considering the time-domain indirect method, the use of an augmented Lyapunov functional is an alternative approach for lowering its inherent conservatism, e.g., in (8), replacing quadratic term x^TPx with $\xi^T(t)P\xi(t)$ yields cross terms about the integral vectors. Therefore, the existing method is unable to deal with weighting matrix P in $\xi^T(t)P\xi(t)$. Thus, an extended symmetry-exploited technique needs to be developed in this paper by further investigating the relationships between the state variables and their integral form.

In Fig.1, ΔP_{vj} and $\Delta P_{vi}, (i \neq j, i, j \in \{1, 2, \ldots, n\})$ have the same relation to Δf. There are some other cases such as $(\Delta f, \Delta P_{mi})$ and $(\Delta f, \Delta P_{mj})$, $(\Delta P_c, \Delta P_{mi})$ and $(\Delta P_c, \Delta P_{mj})$, which has been claimed in [19]. The extended technique is studied assuming that $(\Delta f, \int \Delta P_{mi})$ and $(\Delta f, \int \Delta P_{mj})$ have the same relation. Moreover, the coefficients of $(\int \Delta f, \int \Delta P_{mi})$ and $(\int \Delta f, \int \Delta P_{mj})$ should take identical values. The following descriptions are presented to formalize the above idea.

1) In area i, there are n generation units that constitute a set $\{g_1, g_2, \ldots, g_n\}$. If $g_h, g_k \in \{g_1, g_2, \ldots, g_n\}$, and they have similar structures and parameters for turbines and governors, we let $g_h \sim g_k$ where $\sim$ denotes that there exists an equivalent relationship between generators g_h and g_k.
2) Let $\left\{i_{g_k}^1, \ldots, i_{g_k}^p\right\}$ be the indices of the state variables related to the turbine and governor of generator g_k including ΔP_{mki} and ΔP_{vki}. We define $\mathcal{I}_g = \bigcup_{\forall k,l}\left\{i_{g_k}^l\right\}$ and $\bar{\mathcal{I}}_g$ consisting of the rest of the state variables in the state vector x such as $\Delta f_i, \Delta P_{tie_i,e}$, and $\int y_i$, Then, to deal with the coefficients of the integral terms, in this paper, we add a new set $\left\{\int i_{g_k}^1, \ldots, \int i_{g_k}^p\right\}$, which contains the integral terms of the state variables for the turbine-governor system of the generator g_k. Then, set $\varpi_g = \bigcup_{\forall k,l}\left\{\int i_{g_k}^l\right\}$ is further defined. Meanwhile, $\bar{\varpi}_g$ has the integral terms for $\bar{\mathcal{I}}_g$.
3) In the augmented Lyapunov functional, as the order of matrix P is $(N+1)n_1 + n_2$, we need to preset permutation σ as a bijective map from set $\{1, \ldots, (N+1)n_1 + n_2\}$ to itself. Then, a permutation group $\sum$ is defined as the set of all permutations that satisfy $\sigma(\kappa) = \kappa$ if $\kappa \in \bar{\mathcal{I}}_g \bigcup \bar{\varpi}_g$, and $\forall g_k, \exists g_h \sim g_k$ such that $\sigma\left(i_{g_k}^l\right) = i_{g_h}^l$ or $\sigma\left(\int i_{g_k}^l\right) = \int i_{g_h}^l, \forall 1 \leq l \leq p$.

Overall, compared with the existing method [19], the extended approach has added two extra sets (ϖ_g and $\bar{\varpi}_g$) to include the integral terms of the state variables. Moreover, the original bijective map is based on set $\{1, \ldots, n_1+n_2\}$, while the current bijective map is extended by enlarging set $\{1, \ldots, (N+1)n_1+n_2\}$, where all pairs of the state variables in matrix P can be found.

Therefore, based on the permutation group $\sum$, the equivalent relationship is established between the pairs of the state variables as $(\kappa_1, \upsilon_1) \sim (\kappa_2, \upsilon_2)$ if and only if there exists $\sigma \in \Sigma$ such that $\kappa_2 = \sigma(\kappa_1)$ and $\upsilon_2 = \sigma(\upsilon_1)$.

Here, the concept of the orbit [24] is employed. Under the permutation group Σ, the orbit at which the state variable pair (κ, υ) is located is given as $\mathcal{O}(\kappa, \upsilon) = \{(\sigma(\kappa), \sigma(\upsilon)) | \sigma \in \Sigma\}$. The orbits partition the set where the permutation group operates. That is, set $\{1, \ldots, (N+1)n_1 + n_2\} \times \{1, \ldots, (N+1)n_1 + n_2\}$ is segmented into several orbits. The definitions of different orbits are illustrated in Table II where the upper part is presented in [19] and the subsequent part is proposed in this paper to investigate the extended symmetry-exploiting technique. Matrices P, Z_i and $U_i, i = 1, 2, \ldots, N$ take same value on each orbit.

Note that the proposed technique is an extended version of [19] since the permutation group $\sum$ is enlarged. Hence, based on this permutation group, we can define orbits for all state variables contained in the Lyapunov functional, i.e., the structures of the weighting matrices P, Z_i and $U_i, i = 1, 2, \ldots, N$ can be restricted according to the rules listed in Table II. Therefore, the number of the decision variables contained in the weighting matrices is reduced, and the numerical tractability of the established LMIs can be strongly improved. By contrast, the technique in [19] can only deal with the weighting matrix P, and moreover, P is subjected to the weighting matrix of the $x^T Px$ term. If the Lyapunov functional contains complicated cross-terms between the normal terms and the integral terms, the existing method cannot address their weighting matrices structurally.

TABLE II
ORBITS DEFINED BASED ON $\sum$ FOR THE PAIR OF STATE VARIABLE (κ, υ)

(κ, υ)	$\mathcal{O}(\kappa, \upsilon)$
$\kappa, \upsilon \in \bar{\mathcal{I}}_g, \bar{\varpi}_g$	$\{(\kappa, \upsilon)\}$
$\left(\kappa, i^l_{g_k}\right), \kappa \in \bar{\mathcal{I}}_g, \bar{\varpi}_g$	$\left\{\left(\kappa, i^l_{g_h}\right) : g_h \sim g_k\right\}$
$\left(i^l_{g_k}, \kappa\right), \kappa \in \bar{\mathcal{I}}_g, \bar{\varpi}_g$	$\left\{\left(i^l_{g_h}, \kappa\right) : g_h \sim g_k\right\}$
$\left(i^{l_1}_{g_k}, i^{l_2}_{g_k}\right)$	$\left\{\left(i^{l_1}_{g_h}, i^{l_2}_{g_h}\right) : g_h \sim g_k\right\}$
$\left(i^{l_1}_{g_k}, i^{l_2}_{g_h}\right), g_k \neq g_h$	$\left\{\left(i^{l_1}_{g_{k'}}, i^{l_2}_{g'_h}\right) : g_{k'} \sim g_k \sim g_{h'} \sim g_h, k' \neq h'\right\}$
$\left(\kappa, \int i^l_{g_{mk}}\right), \kappa \in \bar{\mathcal{I}}_g, \bar{\varpi}_g$	$\left\{\left(\kappa, i^l_{g_{mh}}\right) : g_h \sim g_k\right\}$
$\left(\int i^l_{g_{mk}}, \kappa\right), \kappa \in \bar{\mathcal{I}}_g, \bar{\varpi}_g$	$\left\{\left(i^l_{g_{mh}}, \kappa\right) : g_h \sim g_k\right\}$
$\left(\int i^{l_1}_{g_{mk}}, \int i^{l_2}_{g_{mh}}\right)$	$\left\{\left(\int i^{l_1}_{g_k}, \int i^{l_2}_{g_{mh}}\right) : g_h \sim g_k\right\}$
$\left(\int i^{l_1}_{g_{mk}}, \int i^{l_2}_{g_{mk}}\right)$	$\left\{\left(i^{l_1}_{g_{mh}}, i^{l_2}_{g_{mh}}\right) : g_h \sim g_k\right\}$
$\left(\int i^{l_1}_{g_{mk}}, \int i^{l_2}_{g_{mh}}\right), g_{mh} \neq g_{mk}$	$\left\{\left(i^{l_1}_{g_{k'}}, i^{l_2}_{g'_h}\right) : g_{k'} \sim g_k \sim g_{h'} \sim g_h, k' \neq h'\right\}$

Considering the case of a two-area LFC scheme with $n(n \geq 2)$ generators in each area , we have $x_1 = \left[\Delta f_1, \Delta P_{tie_1,e}, \Delta P_{m11}, \ldots, \Delta P_{mn1}, \int y_1, \Delta f_2, \Delta P_{m12}, \ldots, \Delta P_{mn2}, \int y_2\right]^T$, $x_2 = [\Delta P_{v11}, \ldots, P_{vn1}, \Delta P_{v12}, \ldots, P_{vn2}]^T$. The Lyapunov functional (8) becomes

$$V(t) = \xi^T(t) P \xi(t) + \sum_{i=1}^{2} \int_{t-\tau_i}^{t-\tau_{i-1}} x_1^T(s) U_i x_1(s) ds + \sum_{i=1}^{2} (\tau_i - \tau_{i-1}) \int_{-\tau_i}^{-\tau_{i-1}} \int_{t+\theta}^{t} \dot{x_1}^T(s) Z_i \dot{x_1}(s) ds d\theta. \quad (10)$$

with $\xi^T(t) = \left[x_1^T(t), x_2^T(t), \int_{t-\tau_1}^{t-\tau_0} x_1^T(s) ds, \int_{t-\tau_2}^{t-\tau_1} x_1^T(s) ds\right]$, P, U_1, U_2, Z_1, and Z_2 being matrices to be determined. The weighting matrix P can be represented by

$$P = \begin{bmatrix} P_{11} & P_{12} & P_{13} & P_{14} \\ * & P_{22} & P_{23} & P_{24} \\ * & * & P_{33} & P_{34} \\ * & * & * & P_{44} \end{bmatrix} \quad (11)$$

To illustrate the concept of orbit, the orbits developed to compose the set that $\{1, \ldots, n_1\} \times \{1, \ldots, n_1\}$ are given to deal with the weighting matrix P_{11} of the Lyapunov functional (10). Based on the above descriptions of the sets of $\mathcal{I}_g$, and $\bar{\mathcal{I}}_g$, we have $\mathcal{I}_g = \{3, \ldots, n+2, n+5, \ldots, 2n+4\}$, and $\bar{\mathcal{I}}_g = \{1, 2, n+3, n+4, 2n+5\}$. The following orbits are shown

$$\mathcal{O}_{\kappa 1} \in \{(\kappa_1, 3), \ldots, (\kappa_1, n+2) | \kappa_1 \in \bar{\mathcal{I}}_g\}$$
$$\mathcal{O}_{\kappa 2} \in \{(\kappa_2, n+5), \ldots, (\kappa_2, 2n+4) | \kappa_2 \in \bar{\mathcal{I}}_g\}$$
$$\mathcal{O}_{\kappa 3} \in \{(\kappa_3, \upsilon_3) | \kappa_3 \neq \upsilon_3, \kappa_3, \upsilon_3 \in \mathcal{I}_g\}$$
$$\mathcal{O}_{\kappa 4} \in \{(\kappa_4, \kappa_4) | \kappa_4 \in \mathcal{I}_g\}$$

Six typical matrices in P are structured as described in Tables III, IV, VI, and V, where $[\Delta P_{m1i}, \ldots, \Delta P_{mni}]^T$ and $[\Delta P_{v1i}, \ldots, \Delta P_{vni}]^T$ are simplified with $[P_{mni}]$ and $[P_{vni}]$, respectively; $\int_{t-\tau_1}^{t-\tau_0} x_1(s) ds$ and $\int_{t-\tau_2}^{t-\tau_1} x_1(s) ds$ are represented with $\int_a x_1$ and $\int_b x_1$, respectively. ⓧ denotes that this region has any appropriate dimensional variant matrix but only X decision variables are required, e.g., in Table III, the coefficient matrix of $[P_{mn1}]$ and $[P_{mn1}]$ has two decision variables. Following the rules in Table II, we obtain

$$P_{11}(3,3) = \begin{bmatrix} p_1 & p_2 & \cdots & p_2 \\ & \ddots & \ddots & \vdots \\ p_2 & & p_1 & p_2 \\ \vdots & \ddots & & \ddots \\ p_2 & \cdots & p_2 & p_1 \end{bmatrix}$$

In Table IV, the coefficient matrix of $[P_{mn1}]$ and $\int_a [P_{mn1}]$ has n decision variables, and its structure is restricted as

$$P_{13}(3,3) = \begin{bmatrix} p_1 & \cdots & p_1 \\ p_2 & \cdots & p_2 \\ \vdots & & \vdots \\ p_n & \cdots & p_n \end{bmatrix}$$

It should be noted that based on the rules for orbits established in Table II for the pair of state variable (κ, υ), other matrices P_{14} and P_{24} are restricted to have the same structures as P_{13} and P_{23}, respectively. P_{34} and P_{44} adopt the structures similar to that of P_{33}. U_1, U_2, Z_1, and Z_2 should take the same restrictions as P_{11}.

In this case, by using the extended symmetry-exploiting technique, we restrict the structures of matrices P, U_1, U_2, Z_1, and Z_2 based on the rules given in Table II. By contrast, the existing technique in [19] only shows the rules of orbits that are given in the upper part of Table II, while it lacks the next part for dealing with the coefficients of the augmented integral terms. That is, the original method in [19] can only handle P_{11}, P_{12} and P_{22} in P. Therefore, through the extended method, the number of decision variables is greatly reduced to $16n + 370$ compared to $30n^2 + 146n + 216$ and $40n^2 + 168n + 180$ for the methods of [19] and [22], respectively.

TABLE III
STRUCTURE OF THE INVARIANT MATRICES P_{11} AND P_{12} FOR A TWO-AREA LFC WITH n GENERATORS IN EACH AREA

	P_{11}							P_{12}	
	Δf_1	$P_{tie_1,e}$	$[P_{mn1}]$	$\int y_1$	Δf_2	$[P_{mn2}]$	$\int y_2$	$[P_{vn1}]$	$[P_{vn2}]$
Δf_1	①	①	①	①	①	①	①	①	①
$P_{tie_1,e}$	*	①	①	①	①	①	①	①	①
$[P_{mn1}]$	*	*	②	①	①	①	①	②	①
$\int y_1$	*	*	*	①	①	①	①	①	①
Δf_2	*	*	*	*	①	①	①	①	①
$[P_{mn2}]$	*	*	*	*	*	②	①	①	②
$\int y_2$	*	*	*	*	*	*	①	①	①

The structure-exploiting techniques consist of the improved model reconstruction method and extended symmetry-

TABLE IV
STRUCTURE OF THE VARIANT MATRIX P_{13} FOR A TWO-AREA LFC WITH n GENERATORS IN EACH AREA

P_{13}	$\int_a \Delta f_1$	$\int_a P_{tie_1,e}$	$\int_a [P_{mn1}]$	$\int_a \int y_1$	$\int_a \Delta f_2$	$\int_a [P_{mn2}]$	$\int_a \int y_2$
Δf_1	①	①	①	①	①	①	①
$P_{tie_1,e}$	①	①	①	①	①	①	①
$[P_{mn1}]$	①	①	ⓝ	①	①	ⓝ	①
$\int y_1$	①	①	①	①	①	①	①
Δf_2	①	①	①	①	①	①	①
$[P_{mn2}]$	①	①	ⓝ	①	①	ⓝ	①
$\int y_2$	①	①	①	①	①	①	①

TABLE V
STRUCTURE OF INVARIANT MATRIX P_{33} FOR A TWO-AREA LFC WITH n GENERATORS IN EACH AREA

P_{33}	$\int_a \Delta f_1$	$\int_a P_{tie_1,e}$	$\int_a [P_{mn1}]$	$\int_a \int y_1$	$\int_a \Delta f_2$	$\int_a [P_{mn2}]$	$\int_a \int y_2$
$\int_a \Delta f_1$	①	①	①	①	①	①	①
$\int_a P_{tie_1,e}$	*	①	①	①	①	①	①
$\int_a [P_{mn1}]$	*	*	②	①	①	①	①
$\int_a \int y_1$	*	*	*	①	①	①	①
$\int_a \Delta f_2$	*	*	*	*	①	①	①
$\int_a [P_{mn2}]$	*	*	*	*	*	②	①
$\int_a \int y_2$	*	*	*	*	*	*	①

TABLE VI
STRUCTURE OF INVARIANT MATRIX P_{22} AND VARIANT MATRIX P_{23} FOR A TWO-AREA LFC WITH n GENERATORS IN EACH AREA

	P_{22}		P_{23}							
	$[P_{vn1}]$	$[P_{vn2}]$	$\int_a \Delta f_1$	$\int_a P_{tie_1 e}$	$\int_a [P_{mn1}]$	$\int_a \int y_1$	$\int_a \Delta f_2$	$\int_a [P_{mn2}]$	$\int_a \int y_2$
$[P_{vn1}]$	②	①	①	①	ⓝ	①	①	ⓝ	①
$[P_{vn2}]$	*	②	①	①	ⓝ	①	①	ⓝ	①

exploiting techniques. The former is investigated by exploiting the special characteristic of the delayed LFC scheme with only a small number of states being influenced by remote transmission delays. The latter is proposed based on the similar specifications of power equipment in the same area. If the LFC system has these two features, the proposed approaches will be applicable. Thus, it is still convenient for us to extend the proposed approaches to deal with the system model with increased complexity, e.g., the LFC scheme is equipped with generators installed with reheat turbines, hydro power units, gas generators, etc. A two-area LFC scheme has been taken as an example. One area has generators with reheat turbines, and the other area has hydro power generators. Detailed implementations of the proposed methods refers to Appendix II.

Note that this paper has investigated the generators installed with non-reheat turbines, reheat turbines, and hydro power units. All of these generators have different specifications and structures. Therefore, the proposed method can handle the system with different types of generators in different areas. When the same area has different types of generators, we can classify them into several categories at first. That is, the same type of generators can be grouped into one. In each group, we can use the proposed extended symmetry-exploiting techniques to deal with the related system model.

Moreover, the methodologies are proposed based on the LFC scheme with the thermal power plant. Note that nowadays, some grid codes require wind/solar power generators to participate in the frequency response, and therefore, control methods can be used to enable wind/solar power generators to implement droop and inertia characteristics [29], [30]. Although the frequency control characteristics of wind turbines/solar power generators are different from the non-renewable generators, the method proposed in this paper can be extended to deal with the power system with renewable generators participating in the frequency regulation. The coordination of wind turbines/solar power generators to participate in the frequency regulation requires the communication networks and inevitably introduces time delays. The number of states influenced by these delays is still small, and thus, the model reconstruction technique can be applied to realize the model transformation of the relevant model. In addition, the large number of small capacity but similar type of wind turbines/solar power generators in wind farms/solar farms endows the related system model with group symmetry. The extended symmetry-exploiting techniques can be also applied to deal with such type of power systems.

B. Summary of presented method

We briefly describe the implementation of the method presented in this paper as follows.

*Step*1. Establish system model. The state-space model is recalled in Section II.A for the dynamic closed-loop LFC schemes. An improved reconstruction method for the LFC model is proposed in Section II.B, based on which the stability criterion is established.

*Step*2. Exploit extended symmetry techniques. Determine the equivalence relation among generator units and the permutation group on the indices of state variables and their integral terms. Restrict all weight matrices in the Lyapunov functional with appropriate structures by following the rules listed in Table II.

*Step*3. Verify the computational performance. The enhanced calculation efficiency of the approach proposed in this paper is verified by comparison to using the stability condition based on the existing methods.

*Step*4. Validate the calculation accuracy. Use the MATLAB/YALMIP toolbox to calculate the delay margins for the LFC schemes under different stable criteria. Carry out the simulations to show that this paper calculates delay margins with a small degree of conservatism.

IV. CASE STUDIES

Case studies are performed on single-area and three-area LFC schemes. Assuming each area contains different quantities of generators, quantitative calculations are carried out to show that the technique proposed in this paper produces fewer decision variables to be resolved when compared with the existing time-domain indirect methods of [19] and [22]. The improvement of calculation efficiency is then validated in terms of the time required to calculate the delay margins by comparing among the frequency-domain methods reported in [8], [22], and this paper. Moreover, the delay margins obtained through the proposed technique in this paper and the techniques of [8] and [22] are presented. These results combined with the simulations demonstrate that the novel

TABLE VII
COMPARISONS OF COMPUTATIONAL PERFORMANCE ON SINGLE-AREA AND THREE-AREA LFC WITH NON-REHEAT TURBINES

		NoDVs					Computation time			Solver time	
	n	n_{com1} [22]	n_{com2} [19]	n_{tp}	Ratio1	Ratio2	$T_{fm}(s)$[8]	$T_{com1}(s)$[22]	$T_{tp}(s)$	$t_{com1}(s)$[22]	$t_{tp}(s)$
1-area	10	751	511	64	8.5%	12.5%	3.9	34	6	2	0.4
	20	2586	1696	84	3.2%	5.0%	11	115	13	7	0.8
	50	14691	9451	144	1.0%	1.5%	187	–	76	–	4.5
	100	56866	36376	244	0.4%	0.7%	1540	–	364	–	21
	150	126541	80801	344	0.3%	0.4%	5846	–	1312	–	77
	200	223716	142726	444	0.2%	0.3%	–	–	2122	–	125
3-area	$3*1$	1524	1524	1359	89.2%	89.2%	3000	119	90	7	5
	$3*3$	3921	3684	1512	38.6%	41.0%	–	3918	132	230	8
	$3*10$	21099	18867	1890	9.0%	10.0%	–	–	524	–	31
	$3*50$	381519	334047	3636	1.0%	1.1%	–	–	3233	–	190
	$3*80$	944784	825582	5256	0.6%	0.6%	–	–	6167	–	363
	$3*100$	1459794	1274772	6336	0.4%	0.5%	–	–	11160	–	656

techniques proposed in this paper can achieve obviously computational efficiency improvement at the cost of introducing small conservatism.

The case studies are based on the same calculation environment, i.e., a Win 10 PC equipped with an Intel i5 CPU, a 8GB RAM and a 64-bit operation system, and the same presets of the calculation procedure. The methods are implemented in MATLAB 2018b with the YALMIP toolbox. The parameters of the three-area LFC scheme that contains three generators in each area are given in Appendix III. For the single-area LFC scheme, its typical parametric information refers to the parameters of the first generation located in the control area 1. The actual values for T_g, T_t and R are assumed to be randomly generated in the range of $1 \pm \Delta(\%)$ times the typical values such that different degree of non-symmetry for the LFC scheme is reflected through parameter variation by $\Delta(\%)$. Additionally, participation factors $(\alpha_{1i}, \ldots, \alpha_{ni}) \in [0, 1]$ are randomly selected while setting their sum equal to 1. For the three-area LFC scheme, when each area includes more than three generators, their parametric information is obtained by connecting three single-area power systems. The typical values of areas 1, 2, and 3 are taken from the parameters of the first generator located in control areas 1, 2, and 3, respectively.

A. Computational efficiency improvement

To demonstrate that the technique proposed in this paper enables large-scale LMIs to obtain better numerical tractability than those of the frequency-domain method [8] and time-domain methods [19], [22], two related calculation performance metrics, namely, the number of decision variables and the calculation time, are employed. The models of both the single-area and three-area LFC schemes are considered. The single-area model is tested with the number of generators varying from 10 to 200, respectively. For the three-area system, the maximum number of generators increases to 300, i.e., each area has 100 generators.

First, the following binary search algorithm is recalled from [11] to determine the delay margins using the LMI-based stability criterion. The number of bisections is recorded by $count$. The SEDUMI is employed as the solver to check the feasibility of the LMIs.

The number of decision variables required in this paper, [22] and [19] are denoted as n_{tp}, n_{com1} and n_{com2}, respectively.

Step 1: Preset a search interval $[\tau_s, \tau_e]$ and an accuracy requirement τ_{ac}; $count = 0$;

Step 2: **While** $\tau_e - \tau_s > \tau_{ac}$
$count = count + 1$
$\tau_{set} = (\tau_s + \tau_e)/2$;
if LMIs are feasible $\tau_s = \tau_{set}$; else $\tau_e = \tau_{set}$;end
end

Step 3: Output τ_s, $count$

For the single-area LFC scheme ($n \geq 2$), we have

$$n_{tp} = 44 + 2n$$
$$n_{com1} = 5.5n^2 + 18.5n + 16$$
$$n_{com2} = 3.5n^2 + 13.5n + 26$$

Considering the three-area LFC scheme ($n \geq 2$) yields

$$n_{tp} = 1350 + 54n$$
$$n_{com1} = 139.5n^2 + 640.5n + 744$$
$$n_{com2} = 121.5n^2 + 589.5n + 822$$

They are listed in Table VII. Moreover, the calculation time spent on the determination of the delay margins via the methods in this paper (T_{tp}), [8](T_{fm}), and [22] (T_{com1}) for the single-area and three-area LFC schemes is recorded. In this table, "$-$" indicates that the method requires an unacceptable amount of time to determine the delay margins. Moreover, the average time required for checking the feasibility of the derived LMIs is shown (Solver time).

As observed from Table VII, when the number of control areas is unchanged, the method in this paper is unlikely to lead to pronounced growth in the number of decision variables with an increase in the number of generators. By contrast, there exist sharp increases in the number of decision variables produced by [19] and [22] when an increased number of generator units are assumed in each area. Under the three-area LFC scheme, the method in [22] is unable to resolve the delay margins with acceptable time consumption once each area includes more than three generators. Moreover, the frequency-domain method [8] is extremely time-consuming, even for only one generator contained in each area for the three-area LFC scheme, and it is unable to determine the delay margins for cases with three or more generators. By contrast, the method proposed in this paper still achieves a tractable stability criterion for the system model with 300 generators, even though approximately 11160 s is required for

determining the delay margins. Note that the main objectives of delay-dependent stability analysis are to guide the tuning of the controller gains and to eliminate the negative effect of transmission delays. In most cases, a single computation is enough and therefore, it is acceptable that we spend 656 s to check the feasibility of LMIs for tuning controller gains.

B. Calculation accuracy verification

Here, we seek to demonstrate that the LMIs derived in this paper are unlikely to introduce too much conservatism in comparison with the methods of [8] and [22]. When equipped with different PID-type controllers, the single-area LFC scheme with 5 generators together with the three-area LFC scheme including 3 generators in each area is considered. As mentioned in Section IV.A, the method in [8] becomes ineffective in determining the delay margins for the three-area LFC scheme with 3 generators in each area. Hence, only the single-area system is employed to realize the comparisons among [8], [22] and this paper. For the three-area system, the comparison is given between [22] and this paper. Here, the degree of additional conservatism is defined as

$$\delta_1(\%) = \frac{\tau_{com1} - \tau_{tp}}{\tau_{com1}} \tag{12}$$

$$\delta_2(\%) = \frac{\tau_{fm} - \tau_{tp}}{\tau_{fm}} \tag{13}$$

where τ_{fm}, τ_{com1}, and τ_{tp} represent the delay margins determined by the methods in [8], [22], and this paper, respectively.

1) Single-area LFC scheme: For a single-area LFC scheme with 5 generation units and equipped with different PI-type controllers, the delay margins are calculated using the approaches in [8], [22], and this paper, respectively. System parameters T_g, T_t and R are randomly generated between $1 + 10\%$ and $1 - 10\%$ of the typical values. The results are summarized in Table VIII, where the the degree of additional conservatism introduced by this paper is also given based on (12) and (13).

TABLE VIII
COMPARISON OF DELAY MARGINS ON SINGLE-AREA LFC WITH 5 GENERATOR UNITS

K	$\tau_{tp}(s)$	$\tau_{com1}(s)$	$\tau_{fm}(s)$	$\delta_1(\%)$	$\delta_2(\%)$
[0.05 0.05 0]	30.55	31.81	31.91	4.0%	4.3%
[0.05 0.1 0]	15.25	15.64	15.69	2.5%	2.8%
[0.05 0.15 0]	9.99	10.25	10.28	2.5%	2.8%
[0.1 0.05 0]	29.31	31.29	32.72	6.3%	10.4%
[0.1 0.1 0]	15.14	16.06	16.09	5.7%	5.9%
[0.1 0.15 0]	10.32	10.54	10.55	2.2%	2.2%

From Table VIII, when compared with the accurate frequency-domain method [8], the time-domain method used in this paper will introduce no more than 11% additional conservatism for analyzing the stability of the delayed LFC scheme equipped with different PI controllers. Moreover, compared with that of the time-domain method in [22], the degree of additional conservatism will be decreased to less than 7%.

Additionally, the boundaries of the stability regions based on the delay margins are shown in Fig. 2. For the single-area LFC system equipped with the I controllers whose value ranges from 0.04 to 0.2 by the step of 0.02, the delay margins

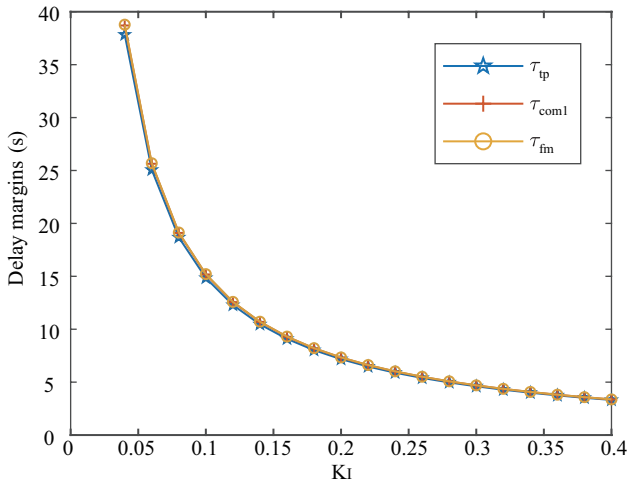

Fig. 2. Stability regions of the single-area LFC obtained by this paper ($\tau_{\rm tp}$), [8] ($\tau_{\rm fm}$), and [22] ($\tau_{\rm com1}$) ($\Delta = 10\%$)

obtained from different methods are decreased. The blue line represents the results obtained through the method proposed in this paper, which always approaches the other two lines that depict the accurate values obtained from the frequency-domain method [8] and the approach in [22], respectively. Thus, the effectiveness of the proposed method in terms of computational accuracy is verified.

For the model of the single-area LFC scheme, the underlying mechanism of the proposed extended symmetry-exploiting technique can be demonstrated by describing the mesh plots of the obtained weighting matrices P, U and Z as shown in Fig.3. The above three sub-figures reveal the weighting matrices calculated by Theorem 1, and the other three pictures describe the structurally restricted matrices $P(\mathcal{O})$, $U(\mathcal{O})$ and $Z(\mathcal{O})$. Due to the similarities between the structures of matrices P, U and Z and those of matrices $P(\mathcal{O})$, $U(\mathcal{O})$ and $Z_2(\mathcal{O})$, it is fair to conclude that the assumption made in Section III.A is appropriate for developing the extended symmetry-exploiting technique.

As the weighting matrices are restricted based on the structure-exploited technique proposed in this paper, the method proposed in this paper inevitably leads to additional conservatism. Here, we need to evaluate the influence that different values of $\Delta(\%)$ have on the conservatism $\delta_2(\%)$ introduced by comparing the delay margins obtained by this paper and [8] for relatively small-scale systems. Obviously, the larger $\Delta(\%)$ is, the more non-symmetric the LFC system is. For a given $\Delta(\%)$, the system parameters are generated randomly from $[1 \pm \Delta(\%)]$ of the typical values. Therefore, to remove the effect of randomness, for each $\Delta(\%)$, the additional conservatism $\delta_2(\%)$ are calculated 20 times. The final $\delta_2(\%)$ is obtained with an average value of 18 times while abandoning the largest and smallest values among the 20 values. When $\Delta(\%)$ increases from 5% to 50%, the variations in $\delta_2(\%)$ are depicted in Fig.4, where the LFC schemes are controlled by different PID controllers.

Based on Fig.4, the additional conservatism $\delta(\%)$ increases with increasing $\Delta(\%)$. Note that even though the degree of non-symmetry increases to 50% and various controllers are

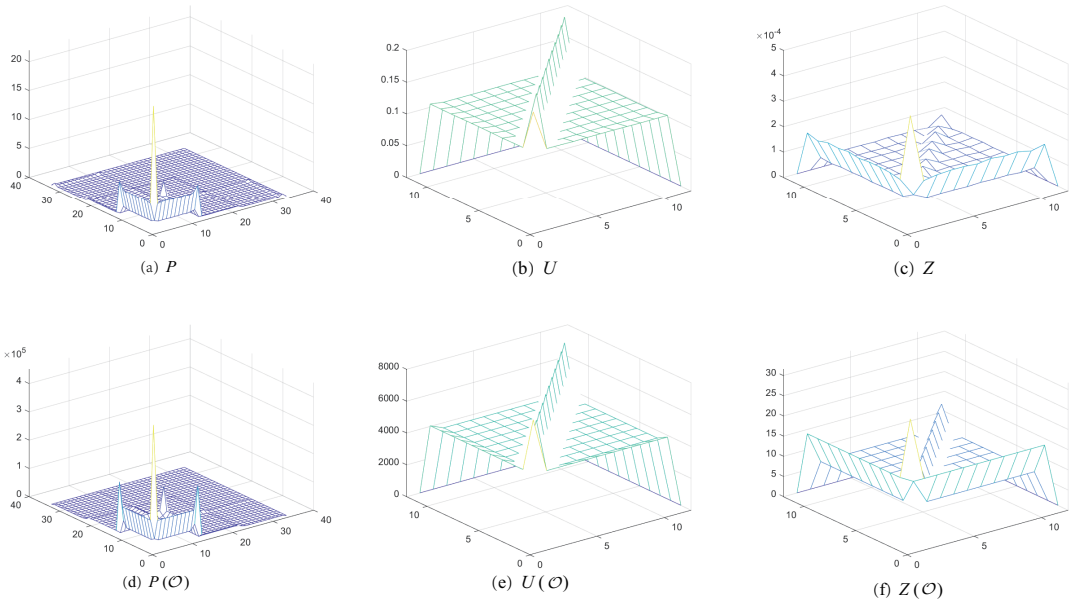

Fig. 3. Comparisons of mesh plots of weighting matrices obtained by Theorem 1 (P,U and Z) and considering symmetry-exploiting technique for Theorem 1 ($P(\mathcal{O})$,$U(\mathcal{O})$ and $Z(\mathcal{O})$) on single-area LFC with 10 generation units.

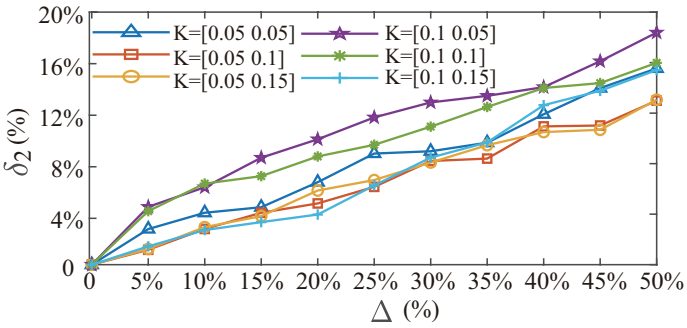

Fig. 4. Degree of additional conservatism $\delta_2(\%)$ of structure-exploiting techniques versus $\Delta(\%)$

utilized, no more than 19% of conservatism will be caused by using the method presented in this paper compared with the result in [22]. Since the proposed LMIs show significant improvement in numerical tractability, the minor cost with respect to accuracy is acceptable.

In addition, as practical power systems contain many generators, e.g., a significant amount of inverter-based renewable generators will be installed in future system, we need to investigate the sensitivity of conservatism to the number of generators. If the proposed techniques bring too much additional conservatism into the stability criterion due to the increased number of generators, these methods will become useless in practice, even though they can achieve greatly improved computational efficiency. We have shown that the degree of non-symmetry of the parameters influences the computational accuracy. Here, we examine the sensitivity of the accuracy reduction by considering $\Delta(\%) \in [5\%, 10\%, 15\%]$, respectively. The number of generators is increased to 100 in steps of 10, and the controller parameter is $K = [0.05, 0.4, 0]$. Thus, the relationship between the additional conservatism $\delta_2(\%)$ and the number of generators n is obtained as shown in Fig. 5.

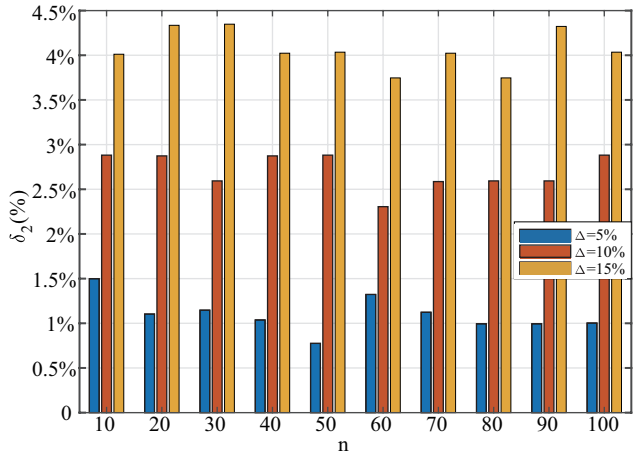

Fig. 5. Degree of additional conservatism $\delta_2(\%)$ of structure-exploiting techniques versus n

It is observed from in Fig. 5 that under the same degree of non-symmetry, the value of $\delta_2(\%)$ fluctuates in a very small range, e.g., for $\Delta(\%) = 5\%$, $\delta_2(\%)$ is always lower than 1.5%, and for $\Delta(\%) = 15\%$, $\delta_2(\%)$ varies from 3.5% to 4.5%. That is, the increased degree of non-symmetry indeed leads to a certain range of additional conservatism, but with an increasing number of generators, there exist no obvious accuracy decreases. Therefore, the proposed method is applicable for the delay-dependent stability analysis of large-scale power systems containing many generators with improved computation efficiency, while the additional conservatism introduced by this method is still acceptable.

In addition, the objective of delay-dependent stability analysis of a delayed LFC system is to accurately estimate the influence of the time delay on system stability in order to

guide the design of controller for the elimination of these adverse effects. Compared with the approaches presented in [22] and [8], the proposed techniques makes a minor sacrifice in accuracy to obtain improved the computational efficiency. To demonstrate the influence of accuracy reduction on guiding controller design and the dynamic performance of the LFC system, the stable regions for the delayed single-area LFC are redescribed in Fig. 6. Based on the stability regions in Fig. 6, given the practical communication delay, we can tune the value of K_I that ensures the stability of the system. Here, we consider that the degree of non-symmetry is $\Delta(\%) = 50\%$ in order to amplify the distinction between the results obtained in this paper, [22], and [8].

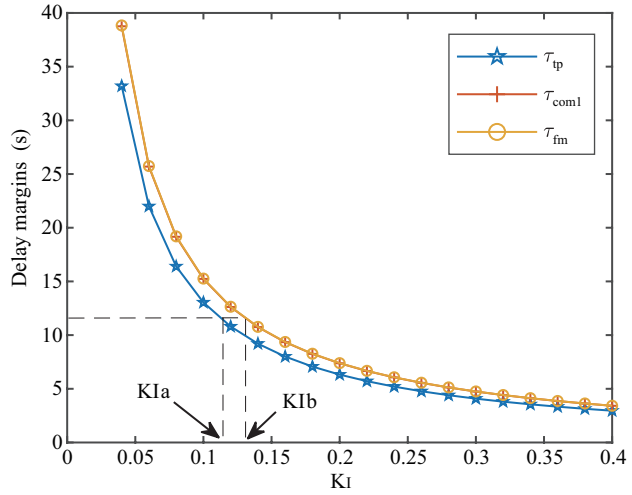

Fig. 6. Stability regions of the single-area LFC obtained by this paper ($\tau_{\rm tp}$), [8] ($\tau_{\rm fm}$), and [22] ($\tau_{\rm com1}$) ($\Delta = 50\%$)

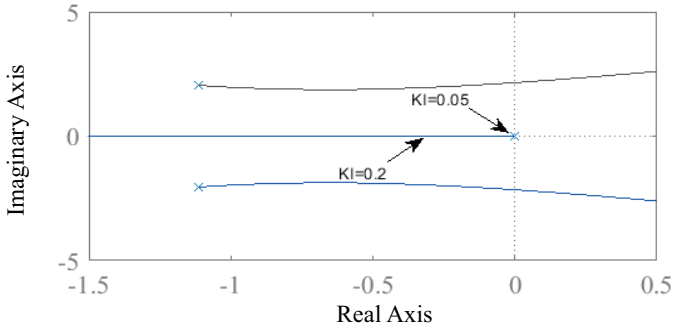

Fig. 7. Root locus of the one-area LFC scheme with $K_P = 0$

The root locus of the closed-loop single-area LFC scheme with respect to K_I is shown in Fig. 7. It is observed that when K_I changes from 0.2 to 0.05, the locations of the complex poles move towards the right half plane, implying that the dynamic performance of the closed-loop system LFC scheme is degraded. Thus, during the design and tuning of the controller, we tend to choose a relatively large gain for K_I. According to Fig. 6, once the time delay is known during the controller design, we obtain $K_I a$ and $K_I b$ based on the stable regions developed by this paper and by the previous methods, respectively. Since the stable region shrinks due to the reduction in the computational accuracy, $K_I a < K_I b$ results in degraded performance of the dynamic LFC scheme.

2) Three-area LFC scheme: The delay margins of a three-area LFC scheme that is controlled with an I-type controller ($K_I = 0.05$), a PI-type controller ($K_P = 0.2, K_I = 0.05$) or a PID-type controller ($K_P = 0.2, K_I = 0.05, K_D = 0.1$) are calculated by employing the LMIs presented in [22] and in this paper, respectively. In these tables, magnitude τ_{tp} (τ_{com1}) and angles ϕ and θ are defined as $\tau_{tp} = \sqrt{\tau_1^2 + \tau_2^2 + \tau_3^2}$, $\phi = \cos^{-1}(\tau_3/\tau_{tp})$ and $\theta = \tan^{-1}(\tau_2/\tau_1)$, respectively.

TABLE IX
DELAY MARGINS DETERMINED BY [22] FOR THE THREE-AREA LFC WITH 3 GENERATOR UNITS IN EACH AREA

$\tau_{com1}(s)$ / $\theta(^\circ)$	$\phi(^\circ)$						
	0	20	40	45	50	70	90
0	30.87	32.91	40.34	43.58	40.36	32.93	30.89
20	30.87	32.91	40.37	43.66	42.99	35.04	32.93
40	30.87	32.90	40.37	43.66	48.09	42.99	40.36
45	30.87	32.90	40.37	43.65	48.08	46.48	43.60
50	30.87	32.90	40.37	43.66	48.09	42.95	40.33
70	30.87	32.91	40.37	43.66	42.94	35.01	32.89
90	30.87	32.91	40.34	43.58	40.33	32.89	30.87

TABLE X
DELAY MARGINS DETERMINED BY THIS PAPER FOR THE THREE-AREA LFC WITH 3 GENERATOR UNITS IN EACH AREA

$\tau_{tp}(s)$ / $\theta(^\circ)$	$\phi(^\circ)$						
	0	20	40	45	50	70	90
0	30.39	32.74	40.22	43.37	40.05	32.80	30.31
20	30.39	32.82	40.37	43.66	42.99	35.03	32.80
40	30.39	32.79	40.32	43.59	48.06	42.96	40.04
45	30.39	32.77	40.29	43.54	47.95	46.23	42.69
50	30.39	32.79	40.32	43.59	48.06	42.66	39.40
70	30.39	32.82	40.37	43.66	42.92	34.76	32.17
90	30.39	32.74	40.21	42.74	39.40	32.16	30.39

TABLE XI
ADDITIONAL CONSERVATISM INTRODUCED BY THE TECHNIQUE PROPOSED IN THIS PAPER COMPARED WITH THAT IN [22]

$\delta_1(\%)$ / $\theta(^\circ)$	$\phi(^\circ)$						
	0	20	40	45	50	70	90
0	1.6%	0.5%	0.3%	0.5%	0.8%	0.4%	1.9%
20	1.6%	0.3%	0.0%	0.0%	0.0%	0.0%	0.4%
40	1.6%	0.3%	0.1%	0.2%	0.1%	0.1%	0.8%
45	1.6%	0.4%	0.2%	0.2%	0.3%	0.5%	2.1%
50	1.6%	0.3%	0.1%	0.2%	0.1%	0.7%	2.3%
70	1.6%	0.3%	0.0%	0.0%	0.1%	0.7%	2.2%
90	1.6%	0.5%	0.3%	1.9%	2.3%	2.2%	1.6%

For simplicity, some typical results obtained for the three-area LFC scheme equipped with an I-type controller are listed, e.g., Table IX shows the allowable delay upper bounds obtained by the method in [22], while Table X displays the delay margins determined by the method in this paper, and the additional conservatism introduced by using the presented technique is shown in Table XI. The stable region based on the data in Table IX is described in Fig. 8 to show the interactions of the time delays between different areas. Moreover, the additional conservatism introduced by the technique proposed in this paper compared with that in [22] is depicted in Fig.9, where Fig.9(a), Fig.9(b) and Fig.9(c) show the LFC systems with I, PI and PID-type controllers, respectively.

Fig.9 reveals that when the I controller is employed, the degree of additional conservatism is less than 3%. For the PI

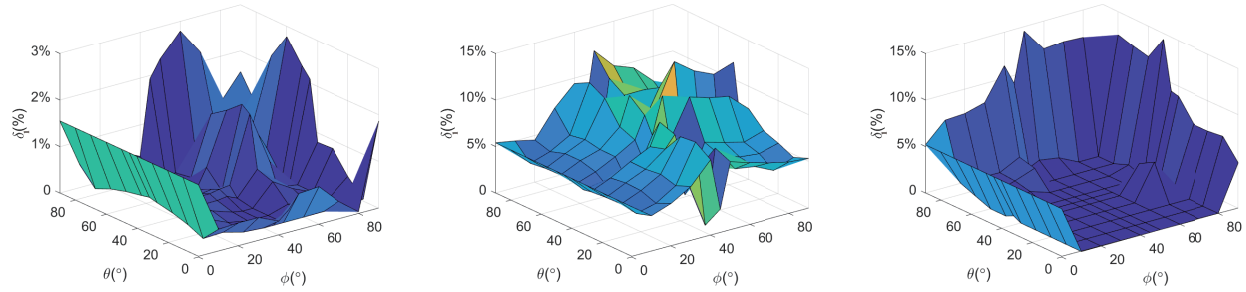

(a) (b) (c)

Fig. 9. Additional conservatism introduced by the technique proposed in this paper compared with that in [22]. (a)$K = [0\ 0.05\ 0]$ (b)$K = [0.2\ 0.05\ 0]$ (c)$K = [0.2\ 0.05\ 0.1]$

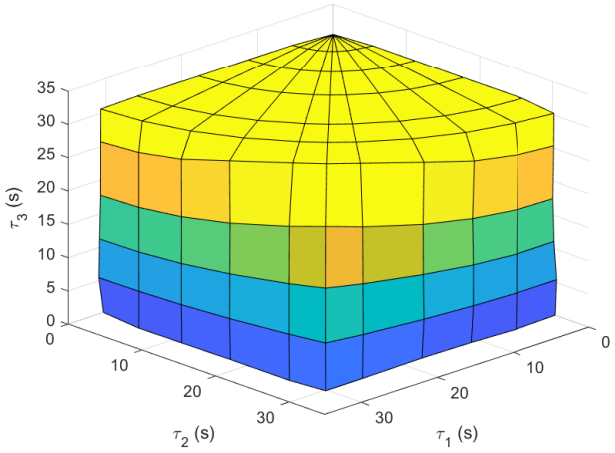

Fig. 8. Stability regions of the traditional three-area LFC obtained by this paper $K = [0\ 0.05\ 0]$

and PID controllers, the values of $\delta(\%)$ do not exceed 15%. In particular, for the system with the PID controller, if all of the delays margins in the three-area LFC scheme are not equal to zero $(\phi, \theta \neq 0°, 90°)$, the conservatism introduced by using the improved structure-exploited technique is decreased.

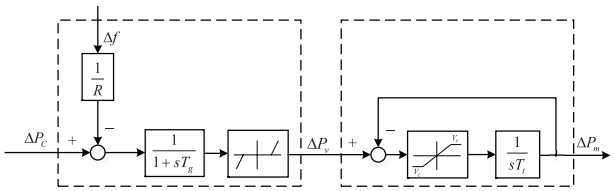

Fig. 10. Structures of GRC and GDB in the LFC scheme.

These results are developed theoretically based on the linear model. To verify that the obtained results are basically consistent with the actual system, simulations are carried out on the three-area LFC diagram with some nonlinearities, including the generation rate constraint (GRC) and the governor dead band (GDB). The diagram is shown in Fig.10 where the GRC is assumed to be ± 0.1 pu/min, and the range of GDB is given as 0.036 HZ [25]. We choose the three-area LFC scheme equipped with I-type controller $(K_I = 0.05)$ and $\phi = 90°$ and $\theta = 50°$. Based on Tables X, we have $\tau_{tp} = 39.4$. Provided that the generation rate constraint is given as ± 0.1 pu/min, and a step load disturbance with 0.1 pu amplitude is assumed (ΔP_{di} =0.1 pu) for each area. First, we assume that transport delays $\tau_{tp} = 39.4$ are induced in the input channel. Then, we gradually increase the time delay to $\tau = 40.5$, enabling the system to be critically stable. The frequency derivations of the three-area LFC scheme are reflected in Fig.12.

Based on Fig. 12, the system responses are asymptotically stable if $\tau_{tp} = 39.4$, i.e., $\tau_1 = 0, \tau_2 = 25.33$, and $\tau_3 = 30.18$, are assumed for the communication channels. The preset of $\tau = 40.5$ leads to the critical stability of the LFC scheme. That is, the actual delay margin is equal to 40.5s, which illustrates that the methods presented in this paper will introduce no more than 3% extra conservatism. Overall, the acceptable sacrifice of calculation accuracy is compensated by the achievement of a clearly improved computation efficiency of large-scale LMIs.

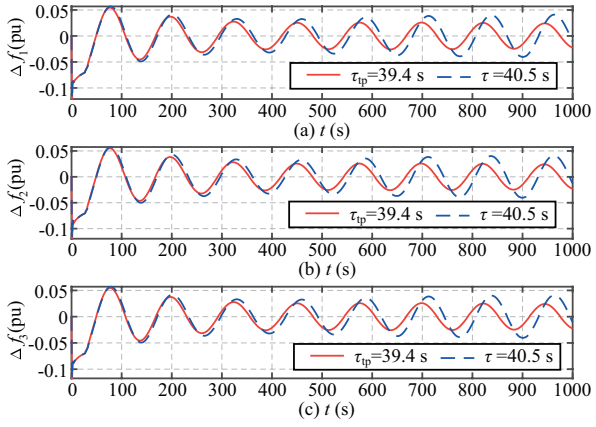

Fig. 12. Responses of three-area LFC scheme with different delays.

To clearly show the underlying mechanism of the proposed extended symmetry-exploiting technique, considering the three-area LFC scheme, the mesh plots of obtained weighting matrices P, U_2 and Z_2 are depicted in Fig. 11. In this figure, Figs. 11(a) to 11(c) display the weighting matrices calculated by Theorem 1 while Figs. 11(d) to 11(f) describe the structurally restricted $P(\mathcal{O})$, $U_2(\mathcal{O})$ and $Z_2(\mathcal{O})$ by the extended symmetry-exploiting technique.

As we can see, the structures of matrices P and Z_2 are similar to those of matrices $P(\mathcal{O})$ and $Z_2(\mathcal{O})$, respectively. It appears that the detailed structures for U_2 and $U_2(\mathcal{O})$ are

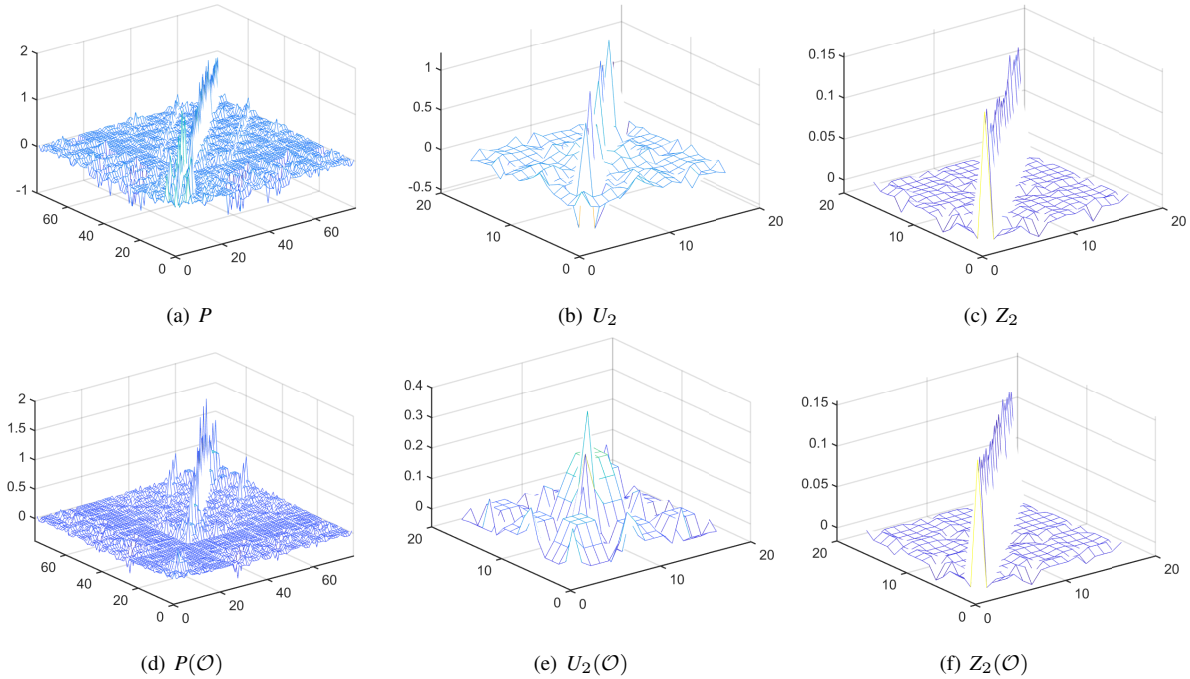

(a) P (b) U_2 (c) Z_2

(d) $P(\mathcal{O})$ (e) $U_2(\mathcal{O})$ (f) $Z_2(\mathcal{O})$

Fig. 11. Comparisons of mesh plots of weighting matrices obtained by Theorem 1 (P,U_2 and Z_2) and considering symmetry-exploiting technique for Theorem 1 ($P(\mathcal{O})$,$U_2(\mathcal{O})$ and $Z_2(\mathcal{O})$) on three-area LFC with 3 generation units in each area.

slightly different. In fact, the parameters of each generator are not completely identical. In Section III.A, we define the orbit where the decision variables in the weighting should take the same value. These restrictions can influence the feasibility of the derived LMIs as well as the obtained values of the weighting matrices. Hence, we need to verify that for most orbits, U_2 has the similar value in each orbit instead of the identical value like $U_2(\mathcal{O})$, as shown in the figures. Therefore, despite the presence of some differences between the obtained weighting matrices, we can still obtain similar values for the delay margins as shown in Section IV.B. That is, the assumption made in Section III.A is reasonable for the development of the extended symmetry-exploiting technique. The establishment of stability criterion based on the improved reconstructed model (6) starts to reduce both the number of decision variables and the order of large-scale LMIs. The computational accuracy of using the time-domain indirect method is guaranteed via an augmented Lyapunov functional. By restricting the structure of the weighting matrices in the augmented Lyapunov functional properly with the extended symmetry-exploiting technique, the calculation burden is further released for the large-scale LMIs while minimizing the conservatism introduced.

3) Multi-machine system: This test system is employed to show that the results based on the linear LFC model (4) are almost consistent with those obtained for an actual power system that has model complexities and nonlinearities. Therefore, the theoretical techniques investigated based on the linear LFC model are verified to be a practical solution for a real-world power system with computational burden. The multi-machine system is based on the 39 bus New England system (NE39) containing 10 units. Larger test systems are constructed by directly scaling up the NE39, i.e., the 100-machine system is obtained by merging 10 NE39 systems [19]. The network topology and parameters of the NE39 refer to those in [26]. The turbine-governor system of each unit is modelled as shown in Fig. 1. The typical values of each turbine governor system are $T_g = 0.08s$ and $T_t = 0.40$, and the droop characteristic R is equal to 5% p.u./rated power. For numerical tests, the actual values of T_g, T_t, and R are randomly given in the range of $1 \pm 10\%$ of the normal values.

Based on the simulation results and the trends of the system responses, the test value of time delay is gradually increased until the response curves tend to be critically stable, and thus, we obtain the real value of the maximum allowable upper bound of time delay (τ_{real}) for the NE39-based multi-machine system. When the scale of the multi-machine system is enlarged by the step of one NE39, its real delay margins are developed. These results are compared with the theoretical delay margins calculated through the proposed methods (τ_{tp}). Fig. 13 shows the comparisons between τ_{real} and τ_{tp} with respect to the number of NE39 (nn). Moreover, the frequency response of the 100-machine power system is depicted in Fig.14 when different time delays are introduced into the communication channel.

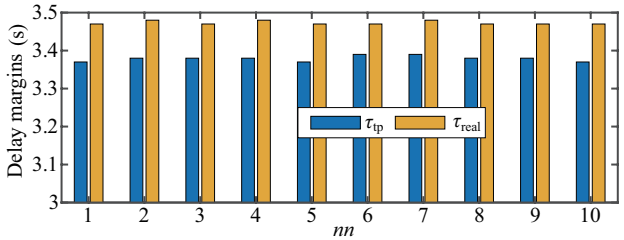

Fig. 13. Delay margins of multi-machine systems obtained by this paper (τ_{tp}) and the real values(τ_{real})

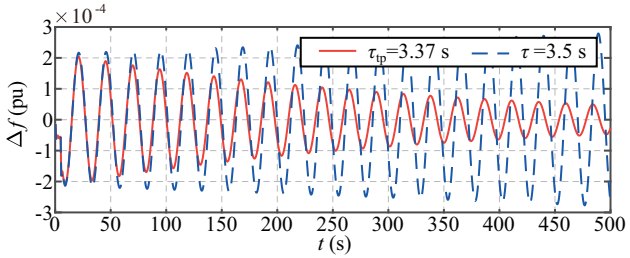

Fig. 14. Responses of 100-machine system with different delays

It is observed from Fig. 13 that there is little difference between τ_{real} and τ_{tp}, even though the scale of the practical system reaches 100 machines, i.e, τ_{real} is always approximately 3.5 s while τ_{tp} approximates 3.4 s. As shown in the time-domain simulation, $\tau_{tp} = 3.37$ is a conservative approximation for the underlying true delay margin, whose value is less than 3.5 s. It can be concluded that this paper presents approaches with less than 4% of conservatism introduced. Therefore, the consistency between the theoretical and practical results is demonstrated. In addition, the proposed method based on the linear large-scale LFC model is beneficial for reducing the computational burden for a real-world power system with numerical difficulties.

V. Conclusion

This paper has investigated the delay-dependent stability analysis of multi-area load frequency control (LFC) schemes based on novel structure-exploiting techniques. The numerical tractability of large-scale linear matrix inequality techniques (LMIs) has been significantly improved. Considering that only a few system states are directly influenced by transmission delays, an improved reconstruction model has been established. Based on this reconstructed model, an augmented-type Lyapunov functional has been employed to develop LMIs with both enhanced computation accuracy and efficiency. Then, via considering the symmetry of the LFC loops, an extended symmetry-exploited technique has been proposed to restrict the structures of the weighting matrices contained in the augmented-type Lyapunov functional such that the numeral tractability of the derived LMIs is further enhanced.

Case studies have been separately carried out on the single and three-area delayed LFC schemes. Comparing with the existing results, the calculation efficiency of large-scale LMIs has been greatly improved via the improved reconstructed method and extended symmetry technique. In addition, the results have shown that the improved numerical tractability has been obtained at the cost of acceptable minor conservatism.

The random parameter variations reflect the different degree of non-symmetry of the power system, and their influence on the conservatism introduced by using structure-exploiting techniques has been investigated in this paper. Note that the derivation of theoretical bounds for the introduced conservatism for a certain class of systems still remains to be investigated in our future work. Besides, the proposed techniques can be used for the controller design of the large-scale delayed power system with significantly improved computational efficiency while guaranteeing that their dynamic performance characteristics will be unchanged. Additionally, as wide-area damping control systems (WADCs) employ only a few remote signals as inputs by using the communication networks, the approaches presented here can be used to investigate the delay-dependent stability analysis and controller design for the WADCs with similar specifications for wide-area power equipment.

Appendix I

Based on the diagram of the LFC scheme, the functions $\lambda(\cdot), h(\cdot), g(\cdot), f(\cdot)$ and $\chi(\cdot)$ employed in Section II.B are defined as the right sides of the following equations, respectively.

$$\Delta\dot{f}_i(t) = \frac{1}{M_i}\left(\sum_{k=1}^{n}\Delta P_{mki}(t) - D_i\Delta f_i(t) - \Delta P_{\mathrm{d}i}(t) - \Delta P_{tie_i,e}(t)\right)$$

$$\Delta\dot{P}_{tie_i,e}(t) = 2\pi \sum_{j=1,j\neq i}^{N} T_{ij}\left(\Delta f_i(t) - \Delta f_j(t)\right)$$

$$\Delta\dot{P}_{mki}(t) = \frac{1}{T_{tki}}\left(\Delta P_{vki}(t) - \Delta P_{mki}(t)\right)$$

$$\Delta\dot{P}_{vki}(t) = \frac{1}{T_{gki}}\left(\frac{1}{R_{ki}}\Delta f_i(t) - \Delta P_{vki}(t) + \alpha_{ki}u(t-\tau_i)\right)$$

where $u(t-\tau_i)$ can be obtained from equations (1) and (2).

The following lemma is recalled for estimating the integral terms contained in the derivative of the Lyapunov functional.

Lemma 1. *[27], [28] For a given matrix $Z > 0$, the following inequality holds for all continuously differentiable functions x in $[a, b] \longrightarrow R^n$:*

$$(b-a)\int_a^b \dot{x}^T(s)Z\dot{x}(s)ds \geq \tilde{\Omega}_1^T Z\tilde{\Omega}_1 + 3\tilde{\Omega}_2^T Z\tilde{\Omega}_2 \qquad (14)$$

where $\tilde{\Omega}_1 = x(b) - x(a)$ and $\tilde{\Omega}_2 = x(b) + x(a) - \frac{2}{b-a}\int_a^b x(s)ds$

Appendix II

This section concerns the two-area LFC schemes: area 1 contains multi-generators with reheat turbines, and area 2 includes hydro power units. By replacing the block diagrams for governors and turbines shown in Fig.1 with Fig. 15, we can obtain the structure of control area $i = 1$. Similarly, the structure of control area $j = 2$ with hydro power units can be obtained by substituting Fig.16 into Fig. 1.

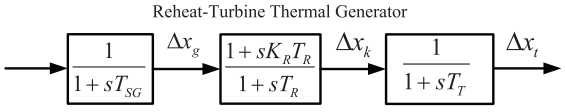

Fig. 15. Diagram of reheat-turbine thermal power plant in control area i

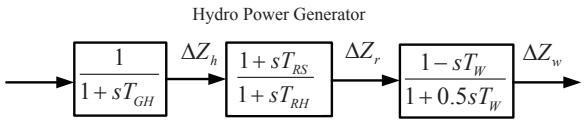

Fig. 16. Diagram of hydro power plant in control area j

The state-space model for each area containing n generators can be derived as follows.

$$\dot{\nu}(t) = \tilde{A}\nu(t) + \tilde{A}_{\mathrm{d}1}\nu(t-\tau_1) + \tilde{A}_{\mathrm{d}2}\nu(t-\tau_2) \qquad (15)$$

TABLE XII
COMPARISONS OF COMPUTATIONAL PERFORMANCE ON TWO-AREA LFC WITH REHEAT TURBINES AND HYDRO-POWER UNITS

		NoDVs					Computation time			Solver time	
	n	n_{com1} [22]	n_{com2} [19]	n_{tp}	Ratio1	Ratio2	$T_{fm}(s)$[8]	$T_{com1}(s)$[22]	$T_{tp}(s)$	$t_{com1}(s)$[22]	$t_{tp}(s)$
2-area	$2*3$	1440	1167	388	26.9%	33.2%	239	27	10	1.8	0.7
	$2*5$	2444	1781	412	16.9%	23.1%	1320	127	19	8.5	1
	$2*10$	6144	3876	472	7.7%	12.2%	–	–	35	–	2
	$2*50$	96944	49436	952	1.0%	1.9%	–	–	558	–	37
	$2*80$	236444	117206	1312	0.6%	1.1%	–	–	1461	–	97
	$2*100$	363444	178386	1552	0.4%	0.9%	–	–	3234	–	216

where

$$\nu = [\bar{\nu}_1^T, \bar{\nu}_2^T], y_i = ACE_i (i = 1, 2)$$

$$\bar{\nu}_1 = [\Delta f_1, \Delta P_{tie_1,e}, \Delta x_{t1}, \ldots, \Delta x_{tn}, \Delta x_{k1}, \ldots, \Delta x_{kn} \quad \Delta x_{g1}, \ldots, \Delta x_{gn}, \int y_1]^T$$

$$\bar{\nu}_2 = [\Delta f_2, \Delta P_{tie_2,e}, \Delta Z_{w1}, \ldots, \Delta Z_{wn}, \Delta Z_{r1}, \ldots, \Delta Z_{rn}, \quad \Delta Z_{h1}, \ldots, \Delta Z_{hn}, \int y_2]^T$$

Detailed information regarding the coefficient matrices $\tilde{A}$, $\tilde{A}_{\mathrm{d1}}$, and $\tilde{A}_{\mathrm{d2}}$ is given in Appendix III.

Based on the reconstructed technique presented in Section II.A, it is found that for the reheat-thermal area, states $[\Delta x_{k1}, \ldots, \Delta x_{kn}, \Delta x_{g1}, \ldots, \Delta x_{gn}]^T$ will be expressed by delayed variables. In the hydro power area, states $[\Delta Z_{w1}, \ldots, \Delta Z_{wn}, \Delta Z_{r1}, \ldots, \Delta Z_{rn}, \Delta Z_{h1}, \ldots, \Delta Z_{hn}]^T$ can be represented by delayed variables. Thus, these two subparts compose the delay-free vector $\nu_2(t) \in R^{m_2}$ in the reconstructed model whose delayed-vector $\nu_1(t) \in R^{m_1}$ consists of the rest of states in $\nu(t) \in R^{m_1+m_2}$. Then, delayed-vector $\nu_1(t)$ is employed to deal with the information of time delay when the Lyapunov functional such as (8) is constructed to derive the delay-dependent stability criterion. By imitating the rules made for the extended symmetry-exploiting techniques in Section III.A, the number of decision variables included in the stability condition can be significantly reduced. As a result, for the two-area LFC system equipped with many hydro power units and thermal generators installed with non-reheat turbines, the calculation burden for analysing its delay-dependent stability can be released.

A. Computational efficiency improvement

We have shown that the technique proposed in this paper enables the numerical tractability of the large-scale power system with generators containing non-reheat turbines. This section aims to verify that the proposed approach can deal with the increasingly complex LFC model. The two-area LFC scheme in which one area is equipped with many re-heated generators and the other area produces hydro power, is taken as an example. The number of generators in the two-area system is up to 200, i.e., 100 generators for the re-heat thermal area and 100 generators for the hydro power area. The number of the decision variables required by the time-domain method in [22], [19], and this paper are calculated, as shown in Table XII. Moreover, this table records the average calculation time required for obtaining the delay margins via the methods proposed in this paper, [8], and [22]. The notations given in this table are defined to be the same as those in Table VII.

Based on Table XII, we can find that due to the increased number of the generators in each area, the numbers of decision variables are significantly increased for the methods in [22] and [19]. The number of decision variables for the latter grows slower than that for the former as the structure-exploiting technique is studied. By contrast, by using the novel structure-exploiting techniques proposed in this paper, the LMI-based stability criterion does not require many decision variables even though the presence of 200 generators in the system model. This paper proposes the method for which the required decision variables are only 0.4% and 0.9% of those required for the approaches reported in [22] and [19], respectively. Moreover, the proposed method can calculate the delay margins within an allowable amount of time despite that there are 200 generators in the LFC scheme. However, the frequency-domain method [8] and time-domain method [22] are unable to derive the delay margins with acceptable time consumption even for a system with only 10 generators in each area. Therefore, the effectiveness of the novel structure-exploiting techniques in computational performance is demonstrated for the LFC system model with increased complexity.

B. Calculation accuracy verification

For a two-area LFC scheme with each area containing 5 generators and equipped with different PI-type controllers, the delay margins are computed by the methods in [8], [22], and this paper, respectively. The system parameters for governors, non-reheat turbines and hydro power generators in the two regions are randomly given in the range $[1 - 10\%, 1 + 10\%]$ of the typical values. The results are listed in Table XIII where $\tau = \sqrt{\tau_1^2 + \tau_2^2}$ represents the magnitude of τ_1 and τ_2 and $\theta = \tan^{-1}(\tau_1/\tau_2)$. Moreover, compared with the existing results, the additional conservatism introduced by this paper is revealed by (12) and (13). The stable boundaries based on delay magnitudes are shown in Fig. 17, where $K_1 = [[0 \ \ 0.05 \ \ 0]]$, $K_2 = [[0 \ \ 0.1 \ \ 0]]$ and $K_3 = [[0 \ \ 0.15 \ \ 0]]$. Note that, as the frequency-domain method [8] can only resolve the system model with equal delays in all areas, for comparison, the data shown in Table XIII are obtained under $\theta = 45^\circ$ In contrast, to describe the stability regions that can clarify the relationship between the different time delays in the two-area LFC scheme, various values for θ are considered. In Fig. 17, the comparisons are performed only between the methods in [22] and this paper.

From Table XIII, the additional conservatism $\delta_2(\%)$ is less than 5% when the comparisons are made between the accurate

TABLE XIII
COMPARISON OF DELAY MARGINS ON TWO-AREA LFC WITH 5 GENERATOR UNITS IN EACH AREA

K	$\tau_{tp}(s)$	$\tau_{com1}(s)$	$\tau_{fm}(s)$	$\delta_1(\%)$	$\delta_2(\%)$
[0 0.05 0]	24.98	25.12	25.35	0.6%	1.5%
[0 0.1 0]	8.34	8.44	8.6	1.2%	3.0%
[0 0.15 0]	3.14	3.23	3.28	2.8%	4.3%
[0.05 0.05 0]	26.34	26.51	26.73	0.6%	1.5%
[0.05 0.1 0]	9.03	9.15	9.22	1.3%	2.1%
[0.05 0.15 0]	3.61	3.69	3.75	2.2%	3.7%

frequency-domain method [8] and the proposed time-domain method. Comparison of the approaches in this paper and [22] shows that the maximum value for additional conservatism $\delta_1(\%)$ is lower than 3%. Fig. 17 reveals that considering the same PI controllers, the stable regions obtained through this paper and the existing results are almost identical. That is, it is fair to conclude that the proposed method incurs only minor conservatism in order to improve the computation efficiency.

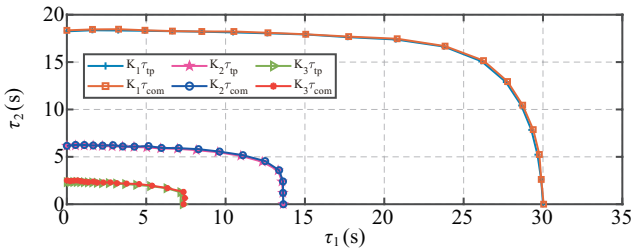

Fig. 17. Stability regions of the two-area LFC obtained by this paper ($\tau_{\rm tp}$) and [22] ($\tau_{\rm com1}$)

To show that the results obtained based on the linear model are reliable in a practical system, for the two-area LFC scheme, simulations are also carried out by taking nonlinearities GRC and GDB into account. Provided that the two-area LFC scheme is equipped with the I-type controller ($K_I = 0.1$) and $\theta = 45°$. Based on Table XIII, we have $\tau_{tp} = 8.34$. When a step load disturbance with 0.1 pu ($\Delta P_{\rm di}$ =0.1 pu) is required for each area, the system responses are recorded in Fig. 18 by considering the induced time delays τ_{tp} and $\tau_{tp} = 8.6$, respectively.

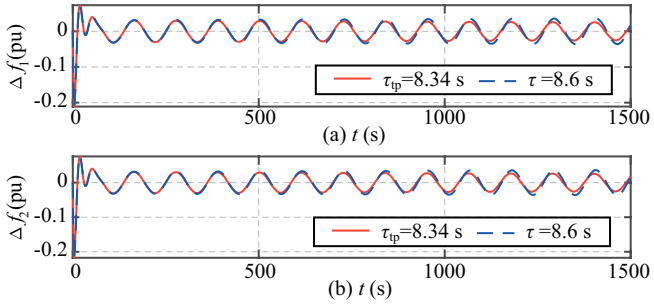

Fig. 18. Responses of two-area LFC scheme with different delays

As we can see, time delay $\tau_{tp} = 8.34$ results in the asymptotical stability of the delayed two-area LFC scheme, while the increase to $\tau = 8.6$ makes the system critically stable. That is, the real value of the delay margins for the practical two-area power system is equal to $\tau = 8.6$, and conservatism introduced by using the theoretical method proposed is less than 3%. Thus, the effectiveness of the presented method in terms of computational accuracy is validated.

APPENDIX III

The parameters for the three-area LFC scheme with each area containing the non-reheat turbines are listed in Table XIV.

TABLE XIV
THREE-AREA LFC SYSTEM AND EACH AREA INCLUDING THREE GENERATORS

	Generators	T_t	T_g	R	D	β	M	α	T_{ij}
Area1	1	0.015	0.1667	0.4	0.08	3	0.3483	0.4	$T_{12}=0.20$
	2	0.014	0.12	0.36	0.06	3	0.3480	0.4	$T_{12}=0.25$
	3	0.015	0.2	0.42	0.07	3.3	0.318	0.2	
Area2	1	0.016	0.2017	0.44	0.06	2.73	0.3827	0.6	$T_{12}=0.20$
	2	0.014	0.15	0.32	0.06	2.67	0.3890	0	$T_{12}=0.12$
	3	0.014	0.1960	0.4	0.08	2.5	0.414	0.4	
Area3	1	0.015	0.1247	0.3	0.07	2.82	0.3692	0	$T_{12}=0.25$
	2	0.016	0.1667	0.4	0.07	3	0.3492	0.5	$T_{12}=0.12$
	3	0.015	0.187	0.41	0.08	2.94	0.355	0.5	

For the two-area LFC scheme, the first area is assumed to contain the re-reheat turbines, and the second area is assumed to include hydro power generators. Their parameters are listed in Table XV.

TABLE XV
TWO-AREA LFC SYSTEM AND EACH AREA CONTAINING ONE GENERATOR

Area1	T_{SG}	K_R	T_R	T_T	R	D	M	T_{ij}
	0.08	0.3	10	0.3	2.4	0.008	0.167	0.545
Area2	T_{GH}	T_{RS}	T_{RH}	T_W	R	D	M	T_{ij}
	48.7	0.6	10	5	1	0.009	0.174	0.545

The detailed information for the coefficient matrices of model (15) is given as follows:

$$\tilde{A} = \begin{bmatrix} \tilde{A}_{11} & \tilde{A}_{12} \\ \tilde{A}_{21} & \tilde{A}_{22} \end{bmatrix}, \tilde{A}_{\rm d1} = \begin{bmatrix} \tilde{A}_{\rm d11} & \tilde{A}_{\rm d12} \\ 0 & 0 \end{bmatrix}, \tilde{A}_{\rm d2} = \begin{bmatrix} 0 & 0 \\ \tilde{A}_{\rm d21} & \tilde{A}_{\rm d22} \end{bmatrix}$$

$$\tilde{A}_{{\rm d}ii} = -\tilde{B}_i K_i \tilde{C}_i, \ \tilde{A}_{{\rm d}ij} = -\tilde{B}_i K_i \tilde{C}_{ij}$$

$$\tilde{A}_{ii} = \begin{bmatrix} \hat{A}_i & 0 \\ \hat{C}_i & 0 \end{bmatrix}, \ \tilde{A}_{ij} = \begin{bmatrix} \hat{A}_{ij} & 0 \\ 0 & 0 \end{bmatrix}, \ \tilde{B}_i = \begin{bmatrix} \hat{B}_i \\ 0 \end{bmatrix}$$

$$\tilde{C}_i = \begin{bmatrix} \hat{C}_i & 0 \\ 0 & 1 \\ \hat{C}_i \hat{A}_i & 0 \end{bmatrix}, \tilde{C}_{ij} = \begin{bmatrix} 0 & 0 \\ 0 & 0 \\ \hat{C}_i \hat{A}_{ij} & 0 \end{bmatrix}$$

$$\hat{A}_1 = \begin{bmatrix} A_{111} & A_{121} & 0 & 0 \\ 0 & A_{221} & A_{231} & 0 \\ A_{311} & 0 & A_{331} & A_{341} \\ A_{411} & 0 & 0 & A_{441} \end{bmatrix}, \hat{A}_{ij} = \begin{bmatrix} 0 & 0 \\ 2\pi T_{ij} & 0 \\ 0 & 0 \end{bmatrix}$$

$$A_{111} = \begin{bmatrix} -\frac{D_1}{M_1} & -\frac{1}{M_1} \\ 2\pi T_{12} & 0 \end{bmatrix}, A_{121} = \begin{bmatrix} \frac{1}{M_1} & \cdots & \frac{1}{M_1} \\ 0 & \cdots & 0 \end{bmatrix}$$

$$A_{221} = -A_{231} = -{\rm diag}\left\{ \frac{1}{T_{T1}}, \cdots, \frac{1}{T_{Tn}} \right\}$$

$$A_{311} = -\begin{bmatrix} \frac{K_{R1}}{R_{TH1} T_{SG1}} & \cdots & \frac{K_{Rn}}{R_{THn} T_{SGn}} \\ 0 & \cdots & 0 \end{bmatrix}^T$$

$$A_{331} = -{\rm diag}\left\{ \frac{1}{T_{R1}}, \cdots, \frac{1}{T_{Rn}} \right\}$$

$$A_{341}=\text{diag}\left\{\frac{1}{T_{R1}}-\frac{K_{R1}}{T_{SG1}},\cdots,\frac{1}{T_{Rn}-\frac{K_{Rn}}{T_{SGn}}}\right\}$$

$$A_{411}=-\begin{bmatrix}\frac{1}{R_{TH1}T_{SG1}} & \cdots & \frac{1}{R_{THn}T_{SGn}}\\ 0 & \cdots & 0\end{bmatrix}^T$$

$$A_{441}=-\text{diag}\left\{\frac{1}{T_{SG1}},\cdots,\frac{1}{T_{SGn}}\right\}$$

$$\hat{B}_1=\left[0,0,0,\frac{\alpha_{11}K_{R1}}{T_{SG1}},\cdots,\frac{\alpha_{1n}K_{Rn}}{T_{SGn}},\frac{\alpha_{11}}{T_{SG1}},\cdots,\frac{\alpha_{1n}}{T_{SGn}}\right]^T$$

$$\hat{C}_1=[\beta_1,1,0],\beta_1=\sum_{j=1}^{n}\frac{1}{R_{1j}}+D_1$$

$$\hat{A}_2=\begin{bmatrix}A_{112} & A_{122} & 0 & 0\\ 0 & A_{222} & A_{232} & 0\\ A_{312} & 0 & A_{332} & A_{342}\\ A_{412} & 0 & 0 & A_{442}\end{bmatrix},\hat{A}_{21}=\begin{bmatrix}0 & 0\\ 2\pi T_{21} & 0\\ 0 & 0\end{bmatrix}$$

$$A_{112}=\begin{bmatrix}-\frac{D_2}{M_2} & -\frac{1}{M_2}\\ 2\pi T_{21} & 0\end{bmatrix},A_{122}=\begin{bmatrix}\frac{1}{M_2} & \cdots & \frac{1}{M_2}\\ 0 & \cdots & 0\end{bmatrix}$$

$$A_{S222}=-A_{S232}=-\text{diag}\left\{\frac{2}{T_{W1}},\cdots,\frac{2}{T_{Wn}}\right\}$$

$$A_{312}=-\begin{bmatrix}\frac{T_{RS1}}{R_{HY1}T_{GH1}T_{RH1}} & \cdots & \frac{T_{RSn}}{R_{HYn}T_{GHn}T_{RHn}}\\ 0 & \cdots & 0\end{bmatrix}^T$$

$$A_{332}=-\text{diag}\left\{\frac{1}{T_{RH1}},\cdots,\frac{1}{T_{RHn}}\right\}$$

$$A_{342}=\text{diag}\left\{\frac{1}{T_{RH1}}-\frac{T_{RS1}}{T_{RH1}T_{GH1}},\cdots,\frac{1}{T_{RHn}}-\frac{T_{RSn}}{T_{RHn}T_{GHn}}\right\}$$

$$A_{412}=-\begin{bmatrix}\frac{1}{R_{HY1}T_{GH1}} & \cdots & \frac{1}{R_{HYn}T_{GHn}}\\ 0 & \cdots & 0\end{bmatrix}^T$$

$$A_{442}=-\text{diag}\left\{\frac{1}{T_{GH1}},\cdots,\frac{1}{T_{GHn}}\right\}$$

$$\hat{B}_2=\left[0,0,\frac{-2\alpha_{21}T_{RS1}}{T_{RH1}T_{GH1}},\cdots,\frac{-2\alpha_{2n}T_{RSn}}{T_{RHn}T_{GHn}},\right.$$
$$\left.\frac{2\alpha_{21}T_{RS1}}{T_{RH1}T_{GH1}},\cdots,\frac{2\alpha_{2n}T_{RSn}}{T_{RHn}T_{GHn}},\frac{\alpha_{21}}{T_{GH1}},\cdots,\frac{\alpha_{2n}}{T_{GHn}}\right]^T$$

$$\hat{C}_2=[\beta_2,1,0],\beta_2=\sum_{j=1}^{n}\frac{1}{R_{2j}}+D_1.$$

REFERENCES

[1] P. Kundur. "*Power System Stability and Control*," New York: McGraw-Hill, 1994.

[2] C. Peng, J. Zhang, "Delay-distribution-dependent load frequency control of power systems with probabilistic interval delays," *IEEE Trans. Power Syst.,* vol. 31, no. 4, pp. 3309-3317, 2016.

[3] J. Nan, W. Yao, J. Wen, et al. "Wide-area power oscillation damper for DFIG-based wind farm with communication delay and packet dropout compensation," *Int. J. Electr. Power Energy Syst.* vol. 124, pp. 106306, 2021.

[4] W. Yao, L. Jiang, J. Wen, et al. "Wide-area damping controller of FACTS devices for inter-area oscillations considering communication time delays," *IEEE Trans. Power Syst.,* vol. 29, no. 1, pp. 318-329, 2014.

[5] C.K. Zhang, L. Jiang, Q.H. Wu, et al. "Delay-dependent robust load frequency control for time delay power systems," *IEEE Trans. Power Syst.,* vol. 28, no. 3, pp. 2192-2201, 2013.

[6] C. Li, J. Wu, C. Duan, et al. "Development of an effective model for computing rightmost eigenvalues of power systems with inclusion of time delays," *IEEE Trans. Power Syst.,* vol. 34, no. 6, pp. 4216-4227, 2019.

[7] S. Sonmez, S. Ayasun, "Stability region in the parameter space of PI controller for a single-area load frequency control system with time delay," *IEEE Trans. Power Syst.,* vol. 31, no. 1, pp. 1-2, 2016.

[8] S. Sonmez, S. Ayasun, C.O. Nwankpa, "An exact method for computing delay margin for stability of load frequency control systems with constant communication delays," *IEEE Trans. Power Syst.,* vol. 31, no. 1, pp. 1-8, 2016.

[9] C. Peng, J. Li, M. Fei, "Resilient event-triggering H_∞ load frequency control for multi-area power systems with energy-limited DoS attacks," *IEEE Trans. Power Syst.,* vol. 32. no. 5, pp. 4110-4118, 2017.

[10] X.C. Shangguan, Y. He, C.K. Zhang, et al. "Switching system-based load frequency control for multi-area power system resilient to denial-of-service attacks," *Control Eng. Pract.,* vol. 107, pp. 104678, 2020.

[11] L. Jiang, W. Yao, Q.H. Wu, et al. "Delay-dependent stability for load frequency control with constant and time-varying delays," *IEEE Trans. Power Syst.,* vol. 27, no. 2, pp. 932-941, 2012.

[12] F. Yang, J. He, D. Wang, "New stability criteria of delayed load frequency control systems via infinite-series-based inequality," *IEEE Trans. Ind. Inf.,* vol. 14, no. 1, pp. 231-240, 2018.

[13] F. Yang, J. He, Q. Pan, "Further improvement on delay-dependent load frequency control of power systems via truncated B-L inequality," *IEEE Trans. Power Syst.,* vol.33, no. 5, pp. 5062-5071, 2018.

[14] C. Peng, J. Zhang, H. Yan, "Adaptive event-triggering H_∞ load frequency control for network-based power systems," *IEEE Trans. Ind. Electron.,* vol. 65, no. 2, pp. 1685-1694, 2018.

[15] C.J. Ramlal, A. Singh, S. Rocke, et al. "Decentralized fuzzy H_∞-iterative learning LFC with time-varying communication delays and parametric uncertainties," *IEEE Trans. Power Syst.,* vol. 34, no. 6, pp. 4718-4727, 2019.

[16] H. Ye, Y. Liu, P. Zhang, "Efficient eigen-analysis for large delayed cyber-physical power system using explicit infinitesimal generator discretization," *IEEE Trans. Power Syst.,* vol. 31, no. 3, pp. 2361-2370, 2016.

[17] H. Ye, Q. Mou, Y. Liu, "Enabling highly efficient spectral discretization-based eigen-analysismethods by Kronecker product," *IEEE Trans. Power Syst.,* vol. 32, no. 5, pp. 4148-4150, 2017.

[18] Y. Li, G. Geng, Q. Jiang, "An efficient parallel Krylov-Schur method for eigen-analysis of large-scale power systems," *IEEE Trans. Power Syst.,* vol. 31, no. 2, pp. 920-930, 2016.

[19] C. Duan, C.K. Zhang, L. Jiang, et al. "Structure-exploiting delay-dependent stability analysis applied to power system load frequency control," *IEEE Trans. Power Syst.,*, vol. 32, no. 6, pp. 4528-4540, 2017.

[20] C.K. Zhang, L. Jiang, Q.H. Wu, et al. "Further results on delay-dependent stability of multi-area load frequency control," *IEEE Trans. Power Syst.,* vol. 28, no. 4, pp. 4465-4474, 2013.

[21] X.D. Yu, H.J. Jia, C.S. Wang, "CTDAE and CTODE models and their applications to power system stability analysis with time delays," *Sci. China Tech. Sci.,* vol. 56, no. 5, pp. 1213-1223, 2013.

[22] L. Jin, C.K. Zhang, Y. He, et al. "Delay-dependent stability analysis of multi-area load frequency control with enhanced accuracy and computation efficiency," *IEEE Trans. Power Syst.,* vol. 34, no. 5, pp. 3687-3696, 2019.

[23] W. Yao, L. Jiang, Q.H. Wu, et al. "Delay-dependent stability analysis of the power system with a wide-area damping controller embedded," *IEEE Trans. Power Syst.,* vol. 26, no. 2, pp. 233-240, 2011.

[24] M. Artin, Algebra, Englewood Cliffs, NJ, USA: Prentice-Hall, 1991.

[25] H. Bevrani. *"Robust power system frequency control,"* New York: Springer, 2009.

[26] T. Athay, R. Podmore, S. Virmani, "A practical method for the direct analysis of transient stability," *IEEE Trans. Power App. Syst.,* vol. PAS-98, no. 2, pp. 573-584, 1979.

[27] A. Seuret, F. Gouaisbaut, "Wirtinger-based integral inequality: Application to time-delay systems," *Automatica*, vol. 49, pp. 2860-2866, 2013.

[28] C.K. Zhang, Y. He, L. Jiang, et al. "Notes on stability of time-delay systems: Bounding inequalities and augmented lyapunov-krasovskii functionals," *IEEE Trans. Automat. Contr.,* vol. 62, no. 10, pp. 5331-5336, 2017.

[29] J.B. Hu, L. Sun, X.M. Yuan, et al. "Modeling of type 3 wind turbines with df/dt inertia control for system frequency response study," *IEEE Trans. Power Syst.,* vol. 32, no. 4, pp. 2799-2809, 2017.

[30] X. Peng, W. Yao, C. Yan, et al. "Two-stage variable proportion coefficient based frequency support of grid-connected DFIG-WTs," *IEEE Trans. Power Syst.,* vol. 35, no. 2, pp. 962-974, 2019.

Li Jin (S-19) received the B.S. degree in automation from China University of Geosciences, Wuhan, China, in 2016 and is pursuing the Ph.D. degree in control science and engineering from China University of Geosciences.

She was a joint Ph.D. student with the Department of Electrical Engineering and Electronics, University of Liverpool, Liverpool, U.K., from 2018 to 2020. Her current research interests include time-delay systems, robust control, power system stability analysis and control.

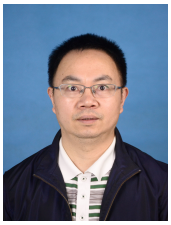

Yong He (SM-06) received the B.S. and M.S. degrees in applied mathematics and the Ph.D. degree in control theory and control engineering from Central South University, Changsha, China, in 1991, 1994, and 2004, respectively.

He was a Lecturer with the School of Mathematics and Statistics, Central South University, and later a Professor with the School of Information Science and Engineering, Central South University, from 1994 to 2014. He was a Research Fellow with the Department of Electrical and Computer Engineering, National University of Singapore, Singapore, from 2005 to 2006, and the Faculty of Advanced Technology, University of Glamorgan, Glamorgan, U.K., from 2006 to 2007. He joined the China University of Geosciences, Wuhan, China, in 2014, where he is currently a Professor with the School of Automation. His current research interests include time-delay systems and networked control systems.

Chuan-Ke Zhang (SM-19) received the B.S. degree in automation and the Ph.D. degree in control science and engineering from Central South University, Changsha, China, in 2007 and 2013, respectively.

He was a Research Associate with the Department of Electrical Engineering and Electronics, University of Liverpool, Liverpool, U.K., from 2014 to 2016. He is currently a Professor with the School of Automation, China University of Geosciences, Wuhan, China. His current research interests include time-delay systems and power systems.

Xing-Chen Shangguan (S-19) received the B.S. degree in automation from China University of Geosciences, Wuhan, China, in 2016 and is pursuing the Ph.D. degree in control science and engineering from China University of Geosciences.

He was a joint Ph.D. student with the Department of Electrical Engineering and Electronics, University of Liverpool, Liverpool, U.K., from 2018 to 2020. His current research interests include sampled-data systems, time-delay systems and power systems.

Lin Jiang (M-00) received his B.S. and M.S. degrees in Electrical Engineering from the Huazhong University of Science and Technology, Wuhan, China, in 1992 and 1996, respectively; and his Ph.D. degree in Electrical Engineering from the University of Liverpool, Liverpool, ENG, UK, in 2001.

He is presently working as a Reader of Electrical Engineering at the University of Liverpool. His current research interests include the optimization and control of smart grids, electrical machines, power electronics and renewable energy.

Min Wu (SM-08/F-19) received the B.S. and M.S. degrees in engineering from Central South University, Changsha, China, in 1983 and 1986, respectively, and the Ph.D. degree in engineering from the Tokyo Institute of Technology, Tokyo, Japan, in 1999.

He was a faculty member of the School of Information Science and Engineering at Central South University from 1986 to 2014, and was promoted to Professor in 1994. In 2014, he joined China University of Geosciences, Wuhan, China, where he is a professor in the School of Automation. He was a visiting scholar with the Department of Electrical Engineering, Tohoku University, Sendai, Japan, from 1989 to 1990, and a visiting research scholar with the Department of Control and Systems Engineering, Tokyo Institute of Technology, from 1996 to 1999. He was a visiting professor at the School of Mechanical, Materials, Manufacturing Engineering and Management, University of Nottingham, Nottingham, U.K., from 2001 to 2002. His current research interests include process control, robust control, and intelligent systems.

Dr. Wu is a Fellow of the IEEE and a Fellow of the Chinese Association of Automation. He received the IFAC Control Engineering Practice Prize Paper Award in 1999 (together with M. Nakano and J. She).